Politecnico di Milano
Department of Mechanical Engineering
Doctoral Programme In Mechanical Engineering

Experimental high resolution analysis of the pressure peaks on a building scale model façades

Doctoral Dissertation of:
Luca Amerio

Supervisor:
Prof. Alberto Zasso
Advisor:
Andrew Allsop
Tutor:
Prof. Stefano Beretta
The Chair of the Doctoral Program:
Prof. Daniele Rocchi

2017 – XXX Cycle

A nonno Angelo

Contents

List of Figures

Abstract

Wind tunnel measurements are an established technique for the assessment of wind induced pressure on building façades. Despite having been used for more than fifty years, there are still some open questions on how to interpret the results of wind tunnel measurements.

Since the Eighties, indeed, as the instrumentation used in the wind tunnels improved, stronger and stronger pressure events have been observed. This growth of the observed peak pressure has been heuristically ascribed to the improvement of the sampling frequency of the equipment. This, along with the fact that no damages had been observed in the buildings designed with the previous lower coefficients, led to the conviction that these stronger events had to be purged from the acquired signal by mean of a low-pass filter.

To support this hypothesis, an equation, the TVL equation, has been proposed to link the duration of the phenomena to their spatial width. Even if this equation has been used for more than forty years, however, very few experimental validations exist in literature.

In this thesis we present an experiment carried out at Politecnico di Milano, in collaboration with the Advanced Technology + Research group of ARUP UK, to experimentally study the validity of the above-mentioned hypothesis. During this experiment, the pressure has been measured on the surface of a prismatic model using extremely closely spaced pressure taps. This allowed to study the spatial distribution of the pressure field and to investigate the relationship between the duration and the width of the dimensioning pressure peaks occurring on the leeward faces of the building.

The results highlight a situation much more complex than the one suggested by the simple TVL equation and raise some doubts regarding its validity. This will be then studied comparing the design value predicted using the time-filtered signals, with the one obtained with the area-averaged signals. The results allow to understand how large is the error performed when using the time-filtered signals in place of area-averaged and to assess which version of

the TVL equation performs best.

The research is then concluded proposing a novel measurement device that could completely overcome the need of an analytical model for the relationship between the time-domain and the space-domain size of pressure phenomena, allowing a *direct* measurement of the area-averaged pressure field.

Sommario

I test in galleria del vento sono una pratica affermata per il calcolo della pressione indotta dal vento sulle facciate degli edifici. Nonostante questa pratica sia in uso ormai da più di cinquant'anni, sussistono ancora degli interrogativi per quanto riguarda l'interpretazione delle misure in galleria del vento.

A partire dagli anni ottanta, infatti, man mano che la strumentazione impiegata nelle gallerie del vento è migliorata, sono stati osservati fenomeni via via più violenti. Questo aumento nel valore di pressione di picco osservato è stato euristicamente attribuito all'aumento della frequenza di acquisizione della strumentazione. Questo, unito al fatto che non erano stati osservati danni negli edifici progettati usando i vecchi coefficienti più bassi, ha portato alla convinzione che il segnale acquisito andasse ripulito da questi eventi più forti per mezzo di un filtro passa-basso.

A supporto di questa ipotesi, una equazione, la TVL equation, fu proposta per collegare la durata dei fenomeni alla loro estensione spaziale. Nonostante questa equazione sia stata utilizzata per più di quarant'anni, esistono pochissime validazioni sperimentali a suo supporto in letteratura.

In questa tesi presentiamo un esperimento condotto al Politecnico di Milano, in collaborazione con il gruppo di Advanced Technology + Research di ARUP UK, per studiare sperimentalmente la validità di tale ipotesi. Durante questo esperimento, la pressione è stata misurata sulla superficie di un modello prismatico usando prese di pressione estremamente ravvicinate. Questo ha permesso di studiare la distribuzione spaziale del campo di pressione ed investigare la relazione tra la durata e la larghezza dei picchi di pressione dimensionanti che avvengono sulle facce sottovento dell'edificio.

I risultati evidenziano una situazione molto più complessa di quella suggerita dalla semplice equazione TVL e sollevano dubbi riguardo la sua validità. Questa verrà poi studiata confrontando il valore di progetto ottenuto usando i segnali filtrati nel dominio del tempo, con quello ottenuto usando i segnali mediati nello spazio. Il risultato ha permesso di capire quanto grande sia l'er-

rore compiuto quando si usano i segnali mediati nel tempo al posto di quelli mediati nello spazio e di capire quale versione della equazione TVL fornisca i risultati migliori.

La ricerca si conclude con la proposta di un innovativo dispositivo di misura che permette di aggirare completamente la necessità di una formulazione analitica per la relazione tra la dimensione dei fenomeni di pressione nello spazio e nel tempo, permettendo una misura diretta del campo di pressione mediato spazialmente.

Chapter 1

Introduction

The accuracy of wind loading calculations has a considerable effect on the sizing of many structural elements. The surface pressures caused by the interaction between the wind and the structure can lead to many different kinds of collapse mechanism, some local and some global. For instance, the external surface pressure can be a major design consideration to determine the glass thickness and glass selection in façades. The recent trend to cover entire buildings, both high-rise and low rise, with glazed façades increased the interest in the calculation of the wind loads on these elements. A façade can be up to 25% of the total cost of a building, being the average cost of a façade approximately $700 per square metre, possibly reaching $2500 per square metre for high specification façades. Thus, a failure can cause considerable economic damages.

In addition, there are various safety implications related to glazing design such as glass breakage due to imposed dynamic pressures or flying debris and the possible domino-effect in façade failure caused by the breakage of a single glass panel. Indeed, wind storms account for about 70% of total insured losses and a direct link is apparent between major storms and worldwide insurance losses from major natural disasters. It is therefore evident that an accurate method for determining wind loading on façades is essential for ensuring a safe and economic glazing design.

In the current state-of-the-art two main possibilities exist for the estimation of the wind design pressure acting on a façade panel: the application of the equations on the national codes of practices or the results of a wind tunnel cladding test. A third possibility that is becoming more attractive in the last decade is the computational simulation of the flow field around the building

using Computational Fluid Dynamic (CFD) techniques. The reliability of the latter used without a backing wind tunnel experiment, however, is a matter of debate and, at the current stage, CFD is seldom used on its own.

For these reasons, when wind-induced pressure is critical for the design of a building - or part of it, such as the cladding system - the current practice is to resort to wind tunnel experiments.

During wind tunnel cladding tests, pressure time histories are recorded in several points across the surface of the building. These time histories are representative of the pressure acting in a (ideally) dimensionless point. For most applications, however, the dimensioning value is the area-averaged one. In the current state-of-the-art this is taken into account multiplying the local pressure spectrum by the "aerodynamic admittance" function.

The experimental evaluation of the admittance function, however, would require the pressure to be measure on a spatially dense array of pressure taps for each area in which a design value is required. In the current wind tunnel commercial practice, the pressure field is measured by means of a number of pressure taps usually in the order of few hundreds (seldom over one thousand) that need to be used to assess the pressure field on the whole surface of a building (that can be tens of thousands square metres). For this reason, it's normal practice to place one pressure tap every 10 square metres or more.

Since the equation of the admittance function is often unknown in wind tunnel tests, Lawson in (Lawson, 1976) and (Lawson, 1980) has suggested to obtain the correct area-averaged pressure filtering the local pressure using a moving average filter with a span equal to:

$$T = KL/V \tag{1}$$

where V is the mean wind speed in a certain reference position, L is a characteristic length of the structure (e.g. the diagonal, the half perimeter or the square root of the area) and K is an arbitrary constant.

The optimal value for the latter has been debated for over three decades. In the original Lawson work (Lawson, 1976) it was assumed to be equal to 4.5 based on full-scale measurement on the Royex House in London. Smaller values have then been proposed by other authors. Greenway in (Greenway, 1979) proposed a value of 1.2 for K. Vickery in (Vickery (1967) cited by Holmes (1997)) proposed a value of $\sqrt{2}$. Finally, Holmes in (Holmes, 1997) proposed to assume $K = 1$. These results were mainly based on the analytical fitting of the aerodynamical admittance function measured by Davenport (and later on by

Vickery and Bearman) at the National Physical Laboratory, for a flat plate. Similar results were also obtained by Newberry in (Newberry et al., 1974) from the full-scale measurement on the façade of the Royex House in London. A better insight into the origin of the TVL equation and it's motivation is discussed in 1.1.

An insight on the available literature, as far as it is known to the authors, shows a lack of experimental studies focused on high space resolution of the pressure distribution for high-rise building façades and on experimental validations of the TVL equation.

Some work has been done by Gavanski and Uematsu (2014) who investigated the spatial distribution of pressure peaks, using an array of 15 x 4 taps recording the pressure on the wall of a low rise building, corresponding to an average distance of 1.5-2 m in full scale. This resolution of pressure taps is considered too coarse to capture concentrated peaks that are at least one order of magnitude smaller. This caused the localized events to be uncorrelated among different taps. Therefore, a proper understanding of the spatial correlation of the peak events is unlikely to be caught.

In addition to this, in the last two decades, the research related to wind peak pressure has been mainly focused on the events occurring behind the leading edge of flat (or nearly-flat) low-rise buildings' roofs. These events has been extensively studied by several authors using either wind tunnel tests (Peng et al., 2014; Banks et al., 2000; Gavanski and Uematsu, 2014; Lin et al., 1995; Lin and Surry, 1998), Computation Fluid Dynamic (Ono et al., 2008) or even full-scale tests (Wu, 2000b,a; Wu et al., 2001; Lin and Surry, 1998).

In particular, Lin and Surry (1998) performed a survey on the effect of area averaging on dimension peak value. This, however, was focused only to the flat-roof corner region. The results are extremely good for the dimensioning of that area, but can be hardly extended to the rest of the building or to high-rise buildings. A similar experiment has been performed by Huang et al. (2014). They proved that the area-averaged peak value on the roof's corners does not depend from the shape of the tributary area. In both papers, the pressure coefficient reduction due to the area-averaging follows a logarithmic decay with respect to the averaging area.

These studies can be used to have a first idea on which could be the phenomena causing strong suction peaks. They, however, are focused on a very specific phenomenon (i.e. the conical vortex on flat roofs). The conclusions of these papers cannot be applied straight forward to all the pressure peaks observed during the wind tunnel tests occurring in areas far from the roof's

edge, such as buildings' lateral surfaces.

In the current wind tunnels practice, however, the pressure time-histories are still either filtered using the methodology suggested by the TVL equation or even with moving-average filter with a span equal to 1 or 3 seconds independently from the value of V or L; even if, to the authors knowledge, no publication exists supporting this method (in Holmes and Allsop (2013) the reason for this habit has been suggested to be related to the response time of typical cup-anemometers, that was used to filter the wind-speed data).

Moreover, the lack of wind tunnel codes of practice makes possible for every wind tunnel to adopt the method it prefers. This is, in the author opinion, one of the possible causes for the large scatter in the results that has been observed in some wind tunnel blind tests.

The pressure time-histories recorded during cladding experiments - especially those occurring on the leeward faces - are characterized by strongly non-Gaussian behaviour and strong negative skewness caused by extreme negative (suction) peaks that can be up to 10-15 standard deviations from the mean value (Rocchi et al., 2010, 2011; Schito et al., 2013). This arises questions regarding the relevance of these peaks for the cladding dimensioning.

The situation gets even worse considering that the extreme value obtained from these time-histories is strongly dependent by the above-mentioned averaging time T used to filter the raw data.

In order to better understand the nature of pressure peaks on the lateral surface an experimental campaign was performed by Politecnico di Milano and ARUP, using closely spaced taps on small areas of a prototype high-rise prismatic building using the highest achievable spatial resolution and highest possible sample rate. The pressure was measured on a 1:50 scale model onto a grid of closely-spaced pressure tap. The research was conducted analysing the pressure in several areas of the building that are usually thought to be the most critical ones.

In this thesis the results of this experimental campaign will be presented and analysed. The purpose is to check the validity of the current state-of-the-art methodology and to produce an insight into the nature of the events that contributes into the cladding designed value measured during experimental tests.

1.1 An insight into the TVL equation story

Since in this thesis we will extensively cite and use the TVL equation as reference and comparison, it is worth to spend few words on its origin and how it has been interpreted by several authors, sometimes drastically changing the meaning of the terms of the equation itself.

The TVL equation has been initially proposed by T.V. Lawson in (Lawson, 1976). In its work, however, Lawson did not provide an extensive derivation of the formula. In its paper he simply stated

> *Newberry et al. have considered the coherence function for full scale measurement over the face of the Royex House and presented these results in graphical form. These can be reproduced to the simple expression $T = 4.5L/V$ where T is the averaging time, L the maximum vertical or horizontal dimension and V is the hourly mean wind speed measured 10m above open flat level country in the vicinity of the site.*

A far deeper insight can instead be found in (Cook, 1985) and (Cook, 1990). Cooks initially introduces the formula in section 8.6.2 of (Cook, 1985) when discussing the overall wind load on buildings. In its work, Cook relates the smallest duration load which acts simultaneously over the structure - the equivalent steady gust duration - to a size parameter and the mean wind speed using the TVL equation. In his review, Cook uses the aerodynamic admittance function to estimate this coefficient. The aerodynamic admittance function $\chi^2(f)$ is analogous to a mechanical frequency response function on an elastic structure and express the relationship between the incoming wind spectrum and the forces acting of the building.

Knowing the admittance function allows to estimate the critical frequency $\bar{f}^*$, where the asterisk indicates the reduced frequency, for which

$$\int_0^{+\infty} \chi^2(f^*)\ \mathrm{d}f^* = \int_0^{\bar{f}^*} 1\ \mathrm{d}f^* \tag{2}$$

In this equation the left-hand side represents the energy introduced in the system by the "real" admittance function, while the right-hand size represents the energy introduced in the system assuming a step-like admittance function from 0 to $\bar{f}^*$.

This kind of admittance function would represent a system where all pressure

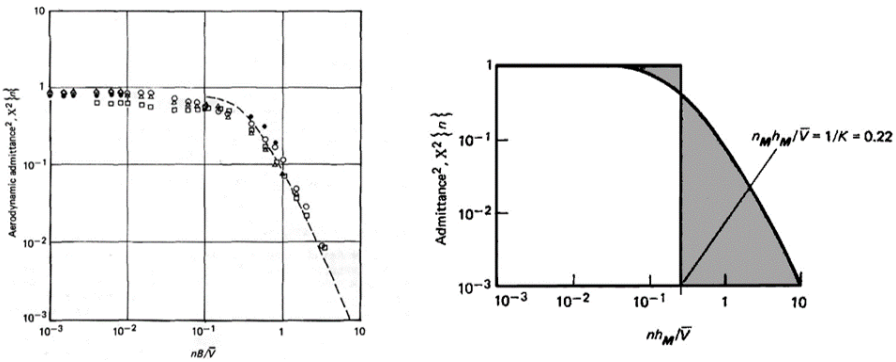

Figure 1: *Left: Aerodynamic admittance for various solid plates (from (Bearman, 1971))*
Right: Graphical representation of equation 2. The two grey zones have the same area (from (Cook, 1985))

fluctuations with a frequency lower than $\bar{f}^*$ are perfectly correlated, whereas all fluctuations at frequencies higher than $\bar{f}^*$ can be ignored.

The admittance function $\chi^2(f^*)$ was firstly estimated in 1961 for a square lattice plate held normal to the flow by Davenport (Davenport, 1961, 1964). Later Davenport investigated the extension of the admittance function to bluff bodies. This was also investigated in 1971 by Vickery and Bearman in the United Kingdom National Physical Laboratory (Bearman, 1971).

The graph on the left in figure 1 shows the admittance function for some Bearman's models results for solid plates of various size and the Vickery's theoretical response. Using the admittance equation found by Vickery and Bearman , Cook estimated the value of $\bar{f}^*$ to be 0.22. This is graphically represented on the right plot of figure 1. Here the Vickery admittance function is compared to a step-like admittance function. The two grey areas represent the energy differences between the two and should be equivalent (note the the plot is in logarithmic scale). This assumption lead to the equation:

$$\bar{f}^* = \frac{fL}{\bar{V}} = 0.22 \quad \Rightarrow \quad t\bar{V} = 4.5L \tag{3}$$

where the time constant t represents the shortest duration load which acts simultaneously over the structure.

In 1997, in (Holmes, 1997), John Holmes performed a review of the TVL equation and compared it to the *analytically* derived admittance function. He based his work on the normalized co-spectrum equation of the pressure fluctuation in two points separated by a distance r, defined as:

$$\gamma(f, r) = \exp\left(-Kfr/\bar{V}\right) \tag{4}$$

This equation can be used to derive the admittance function as:

$$\chi^2(f) = \frac{1}{L} \iint_A \iint_A \gamma(f, \mathbf{x}_1 - \mathbf{x}_2)\ \mathrm{d}\mathbf{x}_1\ \mathrm{d}\mathbf{x}_2 \tag{5}$$

In figure 2 he compared the analytically derived admittance function with the moving average frequency response for different values of K. It is interesting to highlight that the moving average filter proposed by Cook has a reduced cut-off frequency of exactly 0.22 how was originally meant to be. The main problem arose by Holmes is that a moving-average filter has a frequency response function that is far from being step-like. This lead to the major differences highlighted by Holmes and to the conclusions that the optimal value of K should not be 4.5, but 1.

Other authors, such as Greenway in (Greenway, 1979), proposed different interpretations to the TVL. Most of them are however based on the theoretical co-spectrum of pressure, the admittance functions for flat-plates or the wind spectrum. All of these tends to neglect the real geometry of the bluff body and the self-induced turbulence. Moreover, a real experimental study of the admittance function over small portions of a bluff body surface is, to the author's knowledge, never been done.

It is interesting how all the original authors of the TVL equation were somehow critic of its and highlighted how the equation should be used considering its limits. In his original work, Lawson said:

> *Additional evidence is required before this same expression can be used over the short distances covered by cladding panels.*

Cook, instead, in (Cook, 1985, pp. 178) said of the admittance function - that underpin the whole theoretical derivation of the TVL equation:

> *[The way the admittance formula was estimated] leads to the expectation that, while the aerodynamic admittance would not hold for any small area of a large bluff body, it may still be an adequate model for the fluctuations of drag for the whole body*

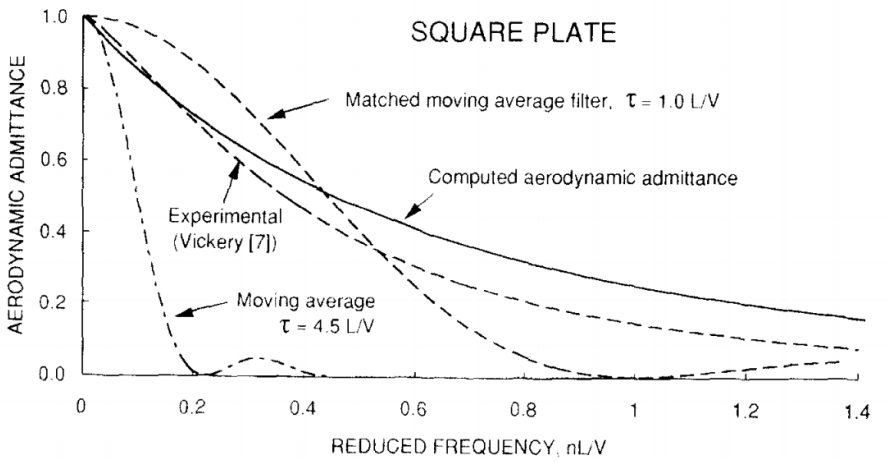

Figure 2: *Comparison of the analytically derived admittance function with the moving average frequency response (from (Holmes, 1997))*

This statement is coherent with the fact that the admittance formula was computed as the frequency response function between the wind spectra and the drag force acting on a body. This should raise doubts regarding the validity of the TVL equation when using a reference length L much smaller than the overall size of the bluff body.

Nonetheless, Cook itself in (Cook, 1990, pp. 22) makes the assumption

> *[...]to limit the duration of the extreme[s] by adopting the time constant t [estimated using the TVL formula]*

when listing the simplifications adopted for the local pressure estimation.

In its 1997 review John Holmes highlighted how in the original Royex House work

> *the value [...] for K has been chosen as an appropriate one for the windward wall, when there are no other buildings upstream. In current usage the same value has been assumed for other building surfaces such as roofs and side walls, although measured values may well be different for these surfaces. This assumption will also be made in this paper.*

This implicitly raise some doubts regarding the validity of this value - and therefore of the underpinned admittance function - for leeward faces of the building. These are however the areas where the strongest negative suction peaks occur and where the use of the TVL equation is more critical.

Another critical aspect in the history of the TVL equation is how the meaning of the variables changed from author to author. Just to cite some examples, in the Lawson work $\bar{V}$ was meant to be the hourly mean wind speed measured 10m above open flat level country. In (Holmes, 1997) $\bar{V}$ is "*the mean wind velocity at some reference point, usually the top of the structure*". Considering an Eurocode category 3 profile, the mean speed at the roof level of a 100m tall building is 65% higher than the mean speed at 10m level.

Also, the meaning of L changes author to author. In the original Lawson paper it was the maximum vertical or horizontal dimension; in (Holmes, 1997) is diagonal of the façade element; while for other authors (e.g. (Greenway, 1979; Lin and Surry, 1998)) it is the square root of the frontal area. For a 2m by 3m façade element, the first is equal to 3m, the second to 3.6m and the latter to 2.4m, leading to an uncertainty in the order of 50%.

Nonetheless, the TVL and the time-filtering techniques are widely adopted in the wind tunnel community. This is probably due to the simplicity of the method and the lack of real alternatives for the wind tunnel pressure signals' analysis.

In this work, when referring to the TVL equation, we will compare our work with the Lawson (or Cook) version adopting $K = 4.5$ and the Holmes version with $K = 1$. For the L value we will adopt the diagonal of the rectangular element, while $\bar{V}$ will be the reference velocity for the test (the same used for the normalization of the pressure value).

Chapter 2

Experimental tests

In the next chapter we will present the experimental campaign held in Politecnico di Milano (hereinafter PoliMi) meant to investigate the real spatial distribution of the peaks and to provide the data for the subsequent analysis. We will introduce the testing procedure, focusing on the description of the model and the test methodology. We will also briefly introduce which test and which data have been collected. The detailed analysis of the results will be performed in chapters 3, 4 and 5.

The main purpose of the test was to study the relationship between the peaks observed in time domain and their spatial extension. This comparison will be used in the following chapter to discuss the correctness of the existing post-processing techniques and to propose a new test methodology.

As already said, it should be noted that these tests were not focused on the understanding of the physical phenomenon (or phenomena) causing these peaks. For this reason, the test focused on the measurement of the pressure field acting on the model surface, rather than the flow-field around the building.

2.1 The wind tunnel

The tests have been carried out in the wind tunnel of PoliMi. This facility is a closed-circuit wind tunnel. The wind tunnel is organized on two floors as can be seen in figure 3. The lower test section has a cross-section equal to $4m \times 4m$ and is dedicated to test that require high-speed ($V_{max} = 55m/s$) and low-turbulence ($I_u < 0.1\%$) such as the aerospace ones. The upper test section, called *Boundary Layer Test Section*, has a cross-section equal to $14m \times 4m$ and a length equal to $35m$. Here the maximum reachable wind speed is equal

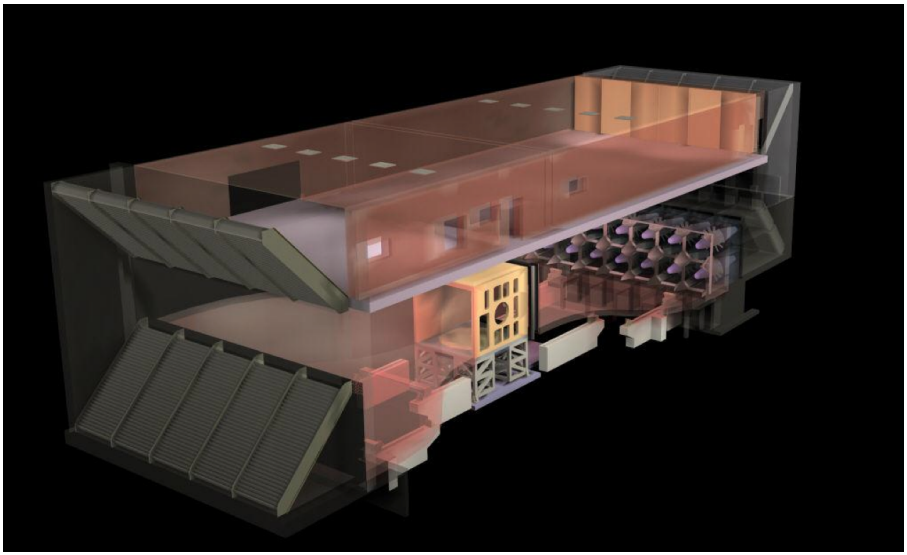

Figure 3: *The PoliMi Wind Tunnel*

to $16m/s$ with a minimum turbulence intensity of about 2%. The wind flow is generated by 14 turbines, each one with a maximum power of 100 kW for a total power of 1.4MW, placed after the high-speed test section. To dissipate the heat generated by the turbines, a heat-exchanger is placed before the boundary layer test section.

The length of the upper test section allows to set up an upstream configuration of active or passive turbulence generators to simulate the atmospheric boundary layer, with turbulence intensity that can be higher than 35%. The model is placed at the centre of a $13m$ diameter rotating table located at the end of the section that allows to simulate different wind directions.

For these tests, the Boundary Layer test section was used.

2.2 Atmospheric Boundary Layer reproduction

The characteristics of the inbound flow strongly affect the pressure distribution acting on the building. This aspect is therefore critical for a good simulation.

Figure 4: *Wind tunnel turbulence generators*

Inside the test section, the Atmospheric Boundary Layer is reproduced using a set of obstacles placed on the floor. In particular two kinds of devices have been used: a group of nine $2.5m$ tall spires placed at the inlet of the test section and a set of concrete bricks covering almost entirely the floor of the test section. (figure 4).

The spires are used to generate the bigger structures and to fasten the creation of the boundary layer. The ground roughness instead slows down the wind near the ground with an effect similar to the buildings and the trees in the real scale scenarios. For this test $60mm \times 100mm \times 200mm$ bricks were used. They were arranged with a staggered array with a distance equal to $1.1m$ both between rows and between elements of the same row.

For this test, the target was an Eurocode Cat. 2 profile. The mean speed

profile is described by the equation:

$$U(z) = U_{ref} log(\frac{z}{z_0}) \tag{6}$$

where z is the height above the ground, U_{ref} is the reference speed for a given site and z_0 is a parameter describing the height at which the mean speed is equal to 0. This latter parameter, called *roughness length* characterize the "shape" of the wind profile. The values of z_0 for each terrain category are provided by the Eurocode. For an open country profile (corresponding to Category 2), the Eurocode prescribe a z_0 equal to $0.05m$. Being a dimensional value, z_0 must be scaled according to the geometric scale chosen for the test.

In current practice, the pressure results are frequently presented as *pressure coefficients*. These are obtained diving the measured pressure by the free-stream dynamic pressure equal to $^1/_2\rho U_{ref}^2$ and are assumed to be almost independent from U_{ref}.

2.2.1 Profile measurement

To verify that the generated profile coincides with the target one, it has to be measured and classified. This is done using a *cobra probe* (figure 5). This is a multi-hole probe that, through direct calibration, can measure the three components of the inbound flow in a point.

Acquiring time histories ad different height is possible to characterize the wind profile. At each height the probe acquired a 5 minutes time history to minimize the statistical error. It is worth to be noted that the time histories acquired at different height are not acquired simultaneously. Hence the integral length scales L_u^z, L_v^z and L_w^z cannot be computed. The integral scales L_u^y, L_v^y and L_w^y cannot be computed as well since the probe doesn't moves in the y direction at all. The only integral scales that can be computed are the ones along x, which can be evaluated using the Taylor frozen turbulence hypothesis.

$$\mathbf{U}(x, y, z, t) = \mathbf{U}(x + \bar{u}t, y, z, 0) \tag{7}$$

2.2.2 Wind profiles used for the test

Figure 6 shows the wind profiles used during the wind tunnel tests. The plot on the left represents the mean speed measured at the model location (without the model) normalized with respect to the mean speed at the reference height ($1m$). The dashed line represents the profile prescribed by the Eurocode for a category 2 terrain with $z_0 = 0.05m$. In the middle plot the turbulence intensity

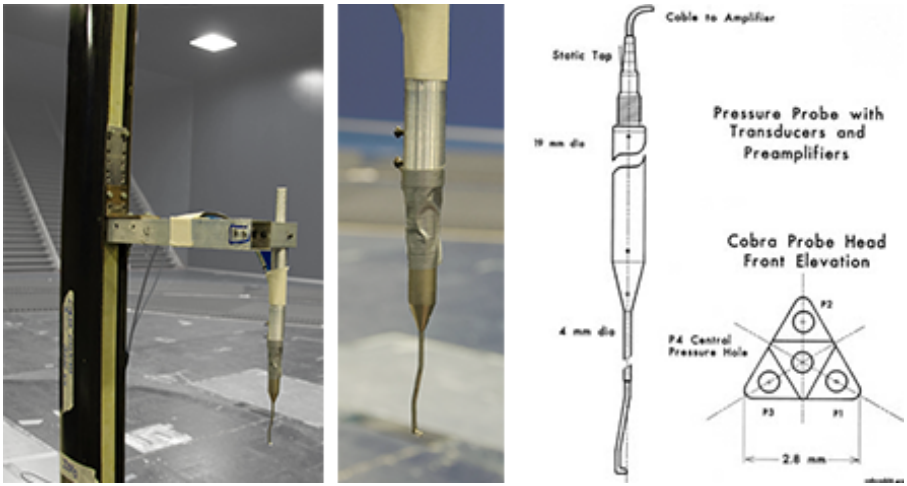

Figure 5: *Cobra probe*

profiles are shown. Again, the dashed lines represent the profiles prescribed by the Eurocode. Lastly, on the right, are presented the integral length scales profiles. These have been calculated fitting the auto-correlation function of the three velocity components using a decaying exponential and integrating them from 0 to infinity.

The measurements show a good agreement for the mean speed profile with the prescribed value. The turbulence intensity is about $5 - 7\%$ lower than the target profile. This however is supposed to not be critical. Lastly, the integral length scales are about half the value prescribed. The Eurocode would prescribe at $1m$ above the ground a length scale equal to $3m$. Such length scale cannot be reached due to the physical dimension of the wind tunnel section. Previous experience of the author suggests that this should not affect the results of the test.

2.3 Scaling

The length scale has been chosen trying to keep it as big as possible, while at the same time producing the best agreement between the target wind profiles and the wind tunnel ones. A large geometric scale indeed makes it easier to

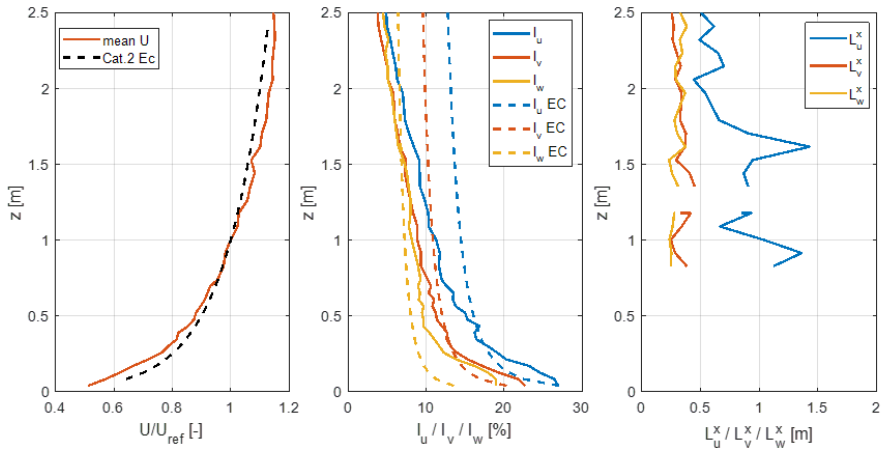

Figure 6: *Wind profiles used for the wind tunnel tests. Left: mean speed profile. Centre: Turbulence intensity. Right: Integral length scales. Dashed lines represent the Eurocode prescribed values for a category 2 terrain*

obtain a smaller full-scale pressure taps distance. Moreover, it helps keeping the Reynolds number of the experiment as high as possible. A length scale of 1:50 produced a good agreement between the two.

The velocity scale was fixed to 1:3. Having a wind-tunnel maximum speed at $1m$ height of $12m/s$, this corresponds to a full-scale wind speed of $36m/s$ that was assumed to be a reasonable reference speed for a normal building with a 50 years return period.

Having fixed the length and the velocity scale, the time scale is just the ratio of the two. This lead to a time scale of about 1:16.6.

2.4 The model

The model used in these tests had the purpose of representing a generic high-rise building. For this reason, the geometry of the model has been kept as simple as possible. The chosen geometry is a rectangular prism with base dimensions equal to $1m \times 0.3m$, model scale, and a height equal to $2m$. Considering a length scale of 1:50, the model is representative of a 100m tall building, being a high-rise, but not exceptional, building. These dimensions,

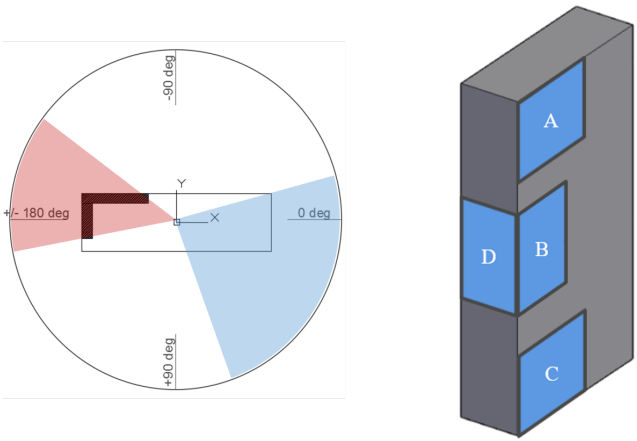

Figure 7: *Tiles position and names*

and in particular the height, were chosen as the biggest ones that could be tested in the PoliMi wind tunnel with a negligible blockage effect. The model was realized with panels of medium density fibreboard (MDF) due to its good smoothness and working easiness. The portions of the model containing the pressure taps instead, were realized using two aluminium tiles. These will be described in the next section. For the sake of keeping the geometry simple, the faces of the model have been kept as smooth and the edges as sharp as possible.

In figure 7 the angle convention is shows as well as the two wind direction ranges investigated.

During the tests, the influence of an upstream building was tested. This secondary building was, again, a rectangular prism, this time with a base dimension equal to $655mm \times 825mm$. The height has been tuned time to time. This will be better described in section 2.4.3.

2.4.1 Pressure taps

Since the purpose of the tests was not to measure the pressure field across the whole building, the taps have been concentrated in a limited set of areas. The tested area are visible in figure 7.

Special care has been put in the making of the portion of surface where the

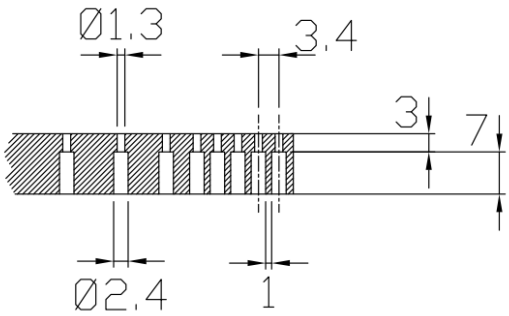

Figure 8: *A section of the aluminium tiles*

taps were placed. In order to achieve to highest taps density and the highest quality, the taps have been placed on two aluminium plates (herein called *aluminium tiles*) realised with a CNC machinery. One tile was used to test position A and C, while the other was used for positions B and D. For the sake of simplicity, hereinafter tiles A and tiles C will be described as two different tiles even if they were the same physical object. The same is true for tiles B and D.

On each tile there were 224 pressure taps. Each pressure tap was made by a hole on the external face of the tile with a diameter equal to $1.3mm$. Corresponding to each hole on the external face, a hole with a diameter of $2.4mm$ was realized on the internal face. Each pressure tap was then connected to the pressure scanner through a rubber tube with an internal diameter of $1.3mm$ and an external one of $2.4mm$. This way there was no discontinuity in the diameter of the air column in the connection between the external hole in the aluminium tile and the tubulation system. A sketch can be seen in figure 8.

On each tile the pressure taps were organized using a grid arrangement with a variable grid step. In each tile an area with the highest achievable taps density was realized. In this area the distance between each row and each column is equal to $3.4mm$. Outside this area the distance between the rows and the columns grows with a geometrical progression. In tiles A and C, the area with the highest density is positioned in a corner, while in tiles B and D it is positioned in the middle of an edge. A sketch of the disposition of the taps on the tiles can be seen in figure 9

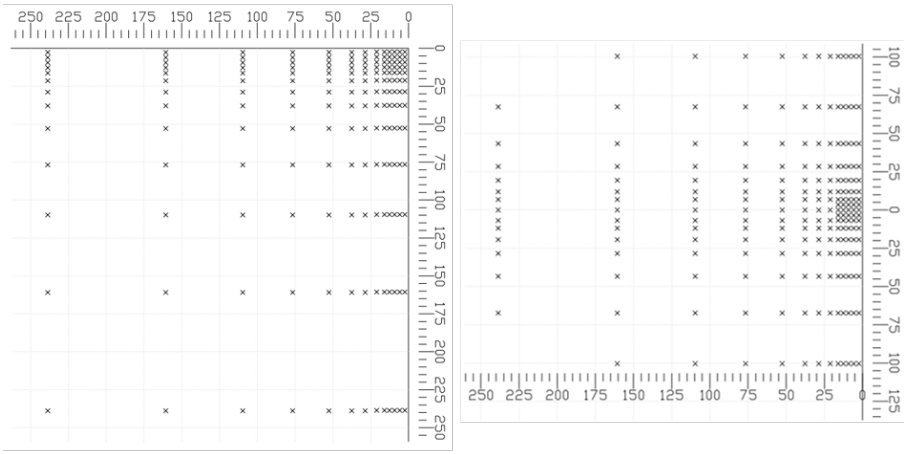

Figure 9: *Position of the taps on tiles A and B. Tile C can be obtained rotating tile A 90 degrees clockwise. Tile D can be obtained rotating tile B 180 degrees.*

In order to maximise the number of pressure taps on the tiles, during each test only one tile was instrumented. As a consequence, the measurement of different tiles is not simultaneous.

In addition to the seven pressure scanner, an eighth scanner was used to measure the pressure across the remaining surface of the building.

2.4.2 Instrumentation and data treatment

The model has been instrumented with 8 PSI ESP-32HD high-speed pressure scanners, each with 32 pressure sensors. The scanners are connected to a Chell QUADdaq data acquisition system that has a sampling frequency equal to 500Hz for each channel. The data are then acquired with a home-made program and stored on file.

Each pressure scanner was connected with a hole on the model surface through a rubber tube. The length of the tubes (except those connected to the eighth scanner) was the same for all the taps and was equal to $500mm$.

During the test a Pitot tube located about $7m$ upwind to the building recorded the flow speed. This data has been used to compute the reference speed for the calculation of the pressure coefficient as will be explained in the next

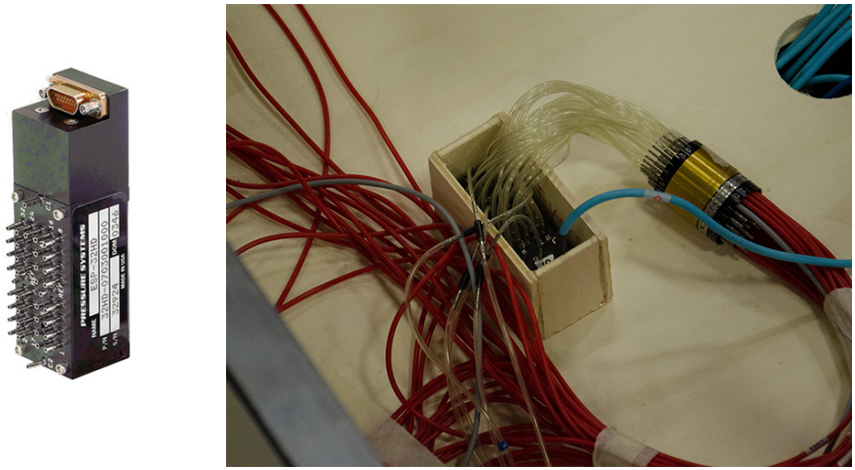

Figure 10: *Left: the Chell ESP-32HD pressure scanner; Right: the pressure scanner and the tubulation system inside the model*

section.

Before doing any analysis, the pressure data have been purged from all the known systematic error or noise. There are mainly two error sources: the distortion of the pressure due to the tubulation system and the acoustic noise generated by the wind tunnel engines. The first has been eliminated dividing the Fourier transform of the signals by the Frequency Response Function of the tubulation system analytically derived and then anti-transforming back in the time domain. A sketch of the tubulation system and the FRF can be seen in figure 11. The latter acoustic noise, instead, has been purged removing from the signals spectra the peaks due corresponding to the analytically computed engines harmonics.

The Chell acquisition system is characterized by the fact that the sampling of the channels is not synchronous. Instead, within each sample time (equal to $1/500s$) the 32 channels are measured sequentially. This asynchrony has been removed when anti-transforming the cleared spectra back in the time-domain.

All the pressure data recorded during the test are herein expressed as *pres-*

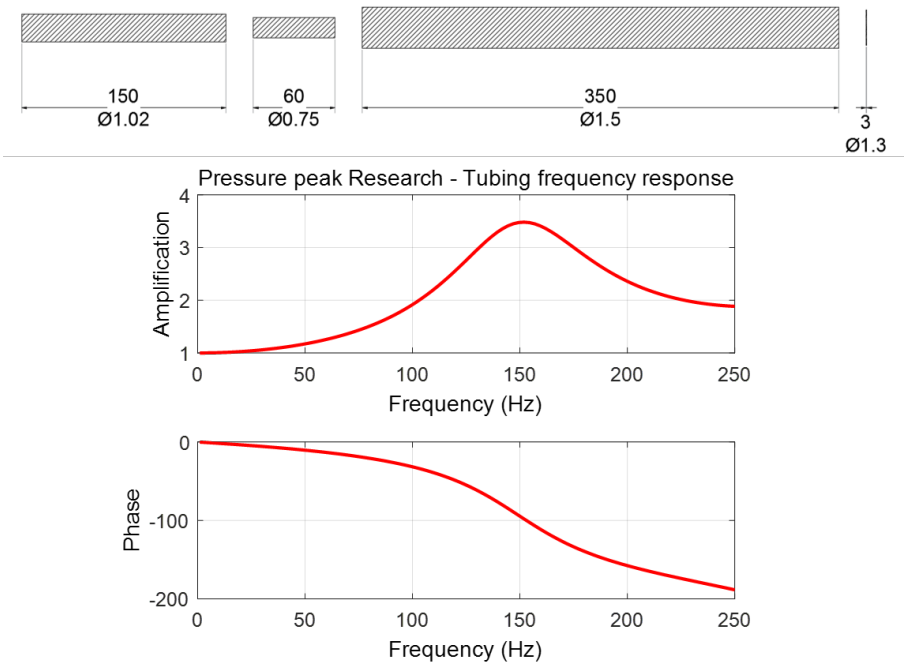

Figure 11: *Top: schematic view of the tubulation cross sections and lengths (units in mm, diameter not to scale). Bottom: frequency response function of the tubulation system.*

sure coefficients. These has been computed with the equation:

$$C_p = \frac{p}{\frac{1}{2}\,\rho\,U_{ref}^2} \tag{8}$$

in this equation U_{ref} is the mean speed measured by the Pitot tube upwind to the model.

2.4.3 Surrounding

During the tests, the influence of a secondary upwind building was studied. The turbulence generated in the shear layer and in the wake of an object presents a correlation much higher than the turbulence that is present in the

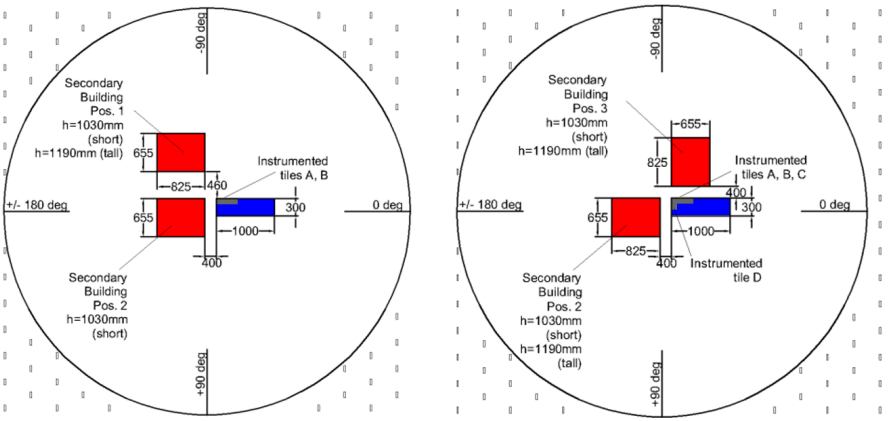

Figure 12: *A scheme representing the position of the secondary building with respect to the main building. They blue rectangle is the main building. The greyed areas are the position of the pressure tiles. The red rectangles indicate the tested position of the secondary building.*

atmospheric boundary layer. This can affect the pressure distribution on the tested building. Hence the presence of a secondary building was tested. The position of the building is represented in figure 12. The height of the secondary building was "tuned" in order to have to most adverse pressure peaks in the area of tile B with the highest taps density i.e. at $1m$ height. Such height was found to be equal to $1190mm$.

2.5 Qualitative analysis of the data

In this section we will present the preliminary results obtained from the wind tunnel tests. These are obtained with ordinary analysis technique. In other words, in this section the data will be analysed only in the time domain, ignoring the spatial informations obtainable exploiting the high density distribution of pressure taps. Even if the results obtained are similar to those obtained in many ordinary tests, this will allow to introduce the problem and understand were we should focus our attention. Due to the large number of variables present in this problem it is extremely hard, if not impossible, to produce the plots of chapters 3 and 4 for all wind directions and configurations. For this

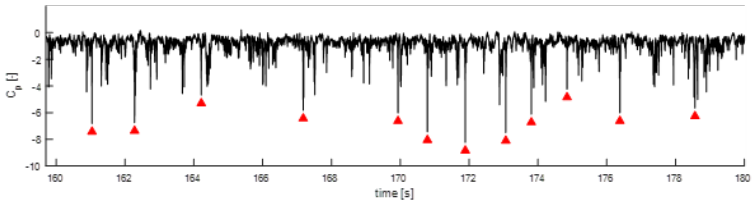

Figure 13: *Time history of a tap close to the building corner. The red arrows show some negative peak events*

reason, in the next section a bulk analysis of the data will be performed and the most significant cases identified. These will be then analysed with greater detail in the following chapters.

2.5.1 Time histories and instantaneous pressure distributions

Figure 13 shows the typical pressure time-history recorded on the leeward face of the model at $\alpha_{exp} = -170$ deg. This exposure is characterised by a large number of very strong peak events as shown in the picture. These events are responsible for the strong non-gaussianity of the probability density function of the pressure value, as can be seen in figure 14.

A great effort was given to assess the physical consistency of the measured very large peak events, but no evidence of any spurious measured peak event was found.

Figure 15-a shows a 0.15s zoom of the time-history, while Figure 10-b represents the instantaneous pressure distribution on Tile A occurring in the instant of most negative C_p (the red spot in Figure 15-a). The application of the peak-extraction method described in section 4 assigns to this event a duration equal to 9.4ms and a width equal to 16.9mm.

This specific event was selected to highlight the physical consistency of the studied peak pressure events, clearly evident in Figure 15, showing an event characterized by short duration and a small width, but at the same time highly correlated on large number of pressure taps.

Figure 16 shows another peak event occurring in the same position. Figure 16-a shows the pressure time history of two taps indicated by the two red circles in Figure 16-b. This event has a duration equal to 4ms and a width equal to 2.5mm. During the event, the 8 taps around the one measuring the event, recorded a pressure reduction between -1.2 and -2.5 C_p.

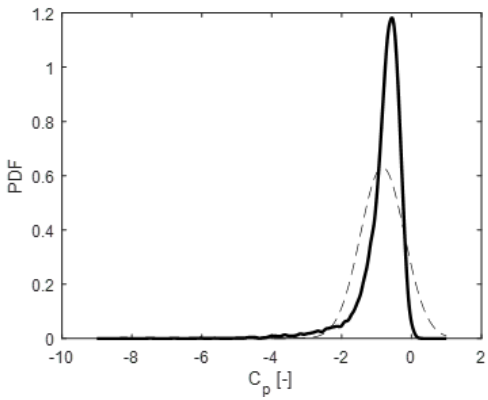

Figure 14: *Probability density function of a tap close to the building corner. The dashed line represents a gaussian PDF with same mean and standard deviation for comparison*

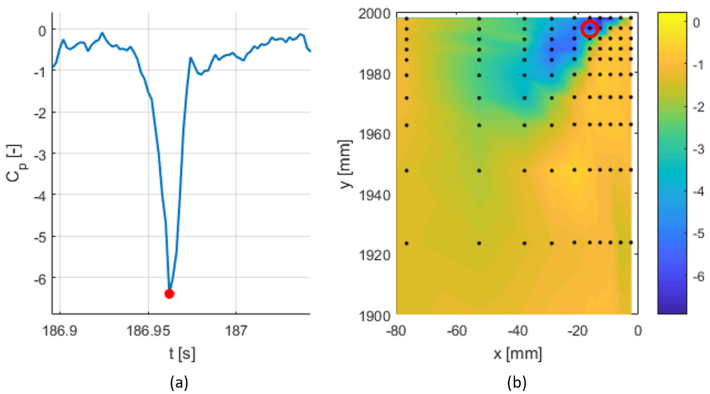

Figure 15: *a) C_p time history, the red dot indicates the instant of time represented in (b). b) instantaneous pressure distribution on the top corner of time A coloured by C_p. The circle indicates the position of tap shown in (a)*

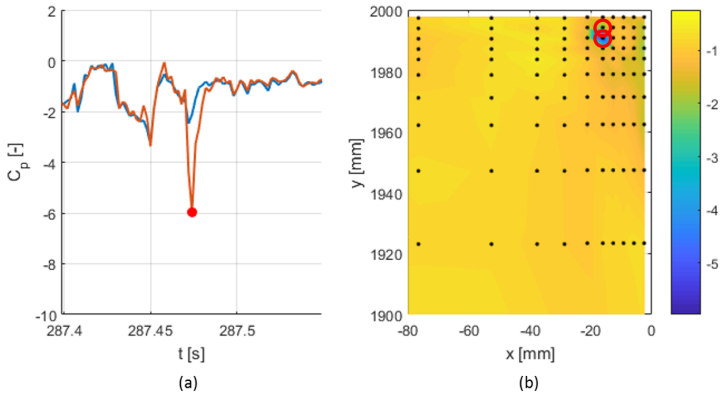

Figure 16: *a) C_p time histories, the red dot indicates the instant of time represented in (b). b) instantaneous pressure distribution on the top corner of time A coloured by C_p. The circle indicates the position of taps shown in (a)*

It is evident how the two events in figure 15 and in Figure 16 has similar duration, but a completely different width.

2.5.2 Polar curves

The first analysis performed on the raw data is the evaluation of the average and expected extreme values (positive and negative) for each pressure tap for each wind direction.

The positive and expected negative extreme values are evaluated using the well-established method described in (Cook, 1985). This method consists in the division of the time-history in 10 minutes (full-scale) intervals. For each interval the maximum (or minimum) value is extracted. These values are then plotted in a double-logarithmic plot and used to fit a Gumbel distribution. A detailed description of the method is beyond the scope of this thesis and can be easily found in (Cook, 1985).

Figure 17 shows the average, positive and negative expected extreme value for each wind direction for four different taps on Tile A evaluated with the Cook & Maine method (Cook and Mayne, 1979; Cook, 1990). The map on the right shows the position of the four considered taps. Each colour correspond to a different tap.

For the wind directions ranging from +140 to +180 and from −180 to −100

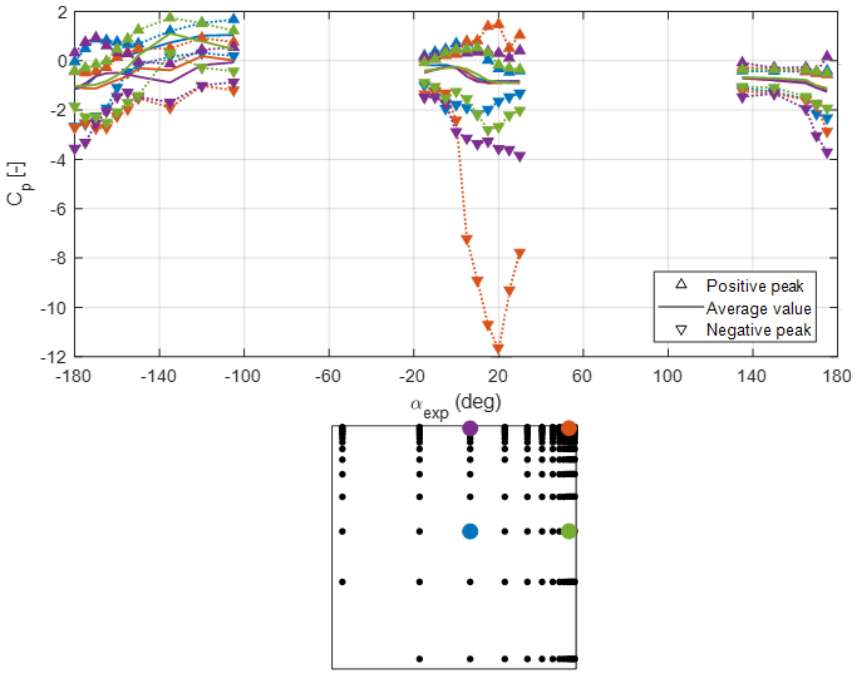

Figure 17: *Polar curve of average and expected maxima/minima value for four pressure taps on Tile A. The colours represent the four different taps visible on the right*

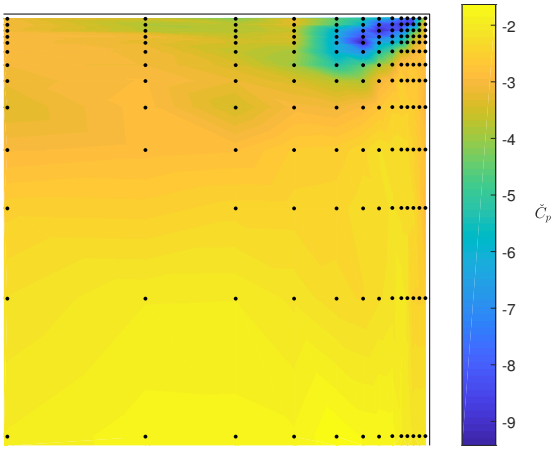

Figure 18: *Map of negative peak pressure on Tile A for* $\alpha_{exp} = 20deg$

degrees, herein *upwind*, the negative peak value is similar for all the four taps, being equal to about $-3 \div -4C_p$. On the other hand, for the exposures ranging from -15 to $+30$ degrees, herein *downwind*, the expected negative value is severely affected by the position. In particular the expected minimum ranges from -2.1, for the tap in the blue position, to -11.8, for the tap in the orange position. For the two wind ranges the most critical angles are: 10 degrees for the *upwind* wind direction range and $+175$ degrees for the *downwind* one; with the latter being the most critical of the two for this area.

Figure 18 shows the expected minimum pressure for the whole Tile A for the case $\alpha_{exp} = 20deg$. It is clear that there is a whole area in the top corner of the building characterized by extreme suction events with peak values exceeding $C_p = 9$. At the same time, the fact that a whole set of taps with a very specific geometric arrangement measured these extreme values, helps to exclude a possible measurement error.

Figure 19 shows the average, positive and negative peak value for each tested wind directions for four taps on Tile B. Again, the expected minimum value for wind directions in the *upwind* configuration is about $-4C_p$. It is still

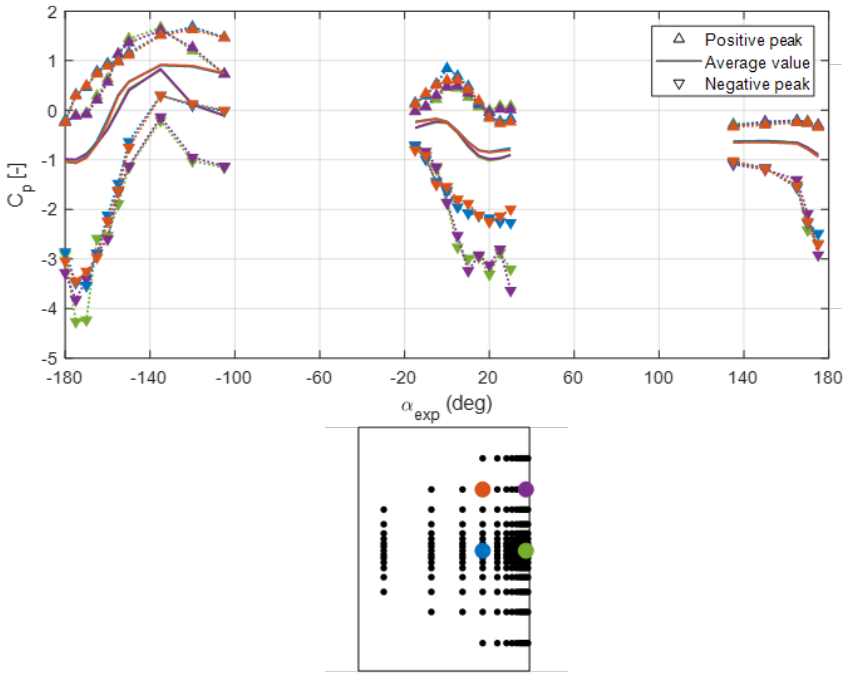

Figure 19: *Polar curve of average and expected maxima value for four pressure taps on Tile B*

possible to identify a local minimum for the wind coming from +10 degrees. This time, however, the peak value is about $-3C_p$ for the taps close to the edge and about -2.5 for the taps farer from it. In this position, therefore, the worst-case scenario is for the wind coming from -175 degrees.

Figure 20 shows the polar curves for the central tap of Tile B with different secondary building configurations. The black line is the stand-alone case and is the same curve in green in figure 19. The other three lines corresponds for three different positions/heights of the upwind building. Since no effect is expected to be caused by a downwind obstacle, only the wind directions from +160 to -160 have been tested. Among these tree configurations, the orange one, corresponding to a building aligned with the tested one, proved to be

the worst case. In this case the peak value dropped to about $-6C_p$, for wind coming from ± 180 degrees.

Figure 21 shows the polar curves for 4 taps on tile C. The peak value for this area is equal to about $-5C_p$ occurring when the tap is close to the windward edge of the building. The peak value is significantly lower for the two taps close to the ground, with the worst area being the one around the purple tap i.e. about $24cm$ from the leading edge.

Lastly, figure 22 shows the pressure coefficient polar curves for Tile D. In this case, since the tile is positioned on the perpendicular face with respect to the other three tiles, it's not surprising that the worst wind directions is equal to -110 degrees. In this case the peak C_p value is equal to about $-7C_p$

The polar curves in the figures from 17 to 22 allow to identify two critical wind directions that are valid for all the configurations for tiles A, B and C. These are -170 degrees for the *upwind* wind directions range, and $+10$ degrees for the *downwind* one. These two wind directions are the ones that will be analysed in greater detail in chapter 3. For tile D the most critical wind direction is -110 degrees. This configurations, however, did not present a behaviour significantly different from the one of tile B and will be therefore ignored in chapter 3. Nonetheless, these data will be used in chapter 4 for the evaluation of the error performed when using the time-filtering techniques.

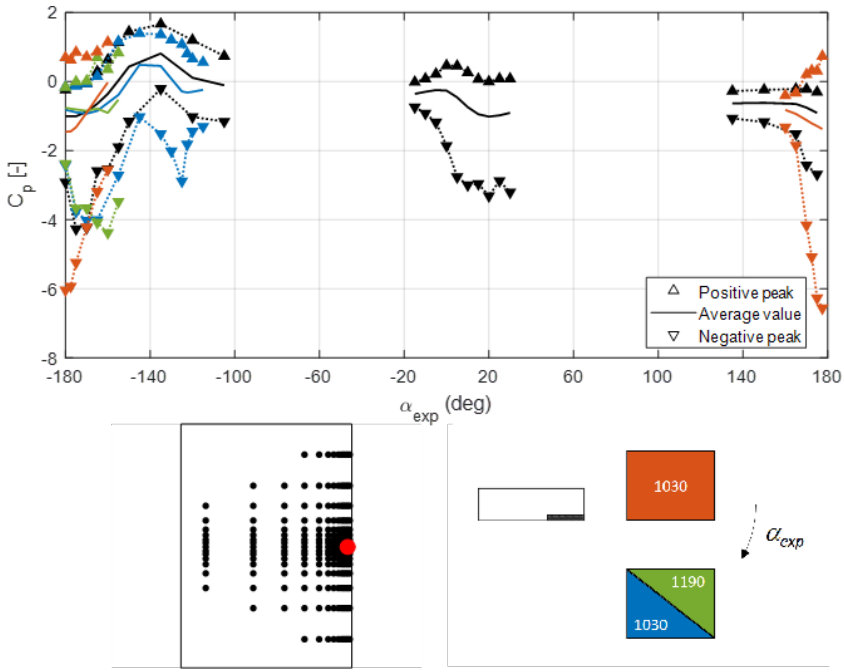

Figure 20: *Polar curve of average and expected maxima value for one pressure taps on Tile B for different secondary building positions. The black curve represents the stand-alone case. The coloured curves correspond to the secondary building position with the same colour shown below. Blue and green curves correspond to the same position, but with different heights. The white number is the height of the secondary building measured in millimetres. The measuring tap is indicated in red in the bottom map and it's 1000 mm from the ground.*

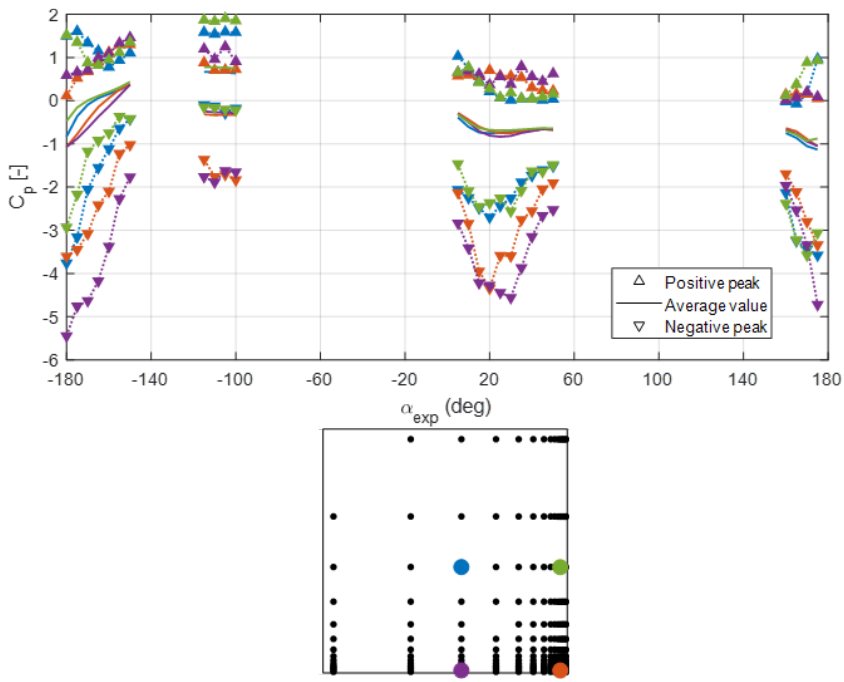

Figure 21: *Polar curve of average and expected maxima value for four pressure taps on Tile C*

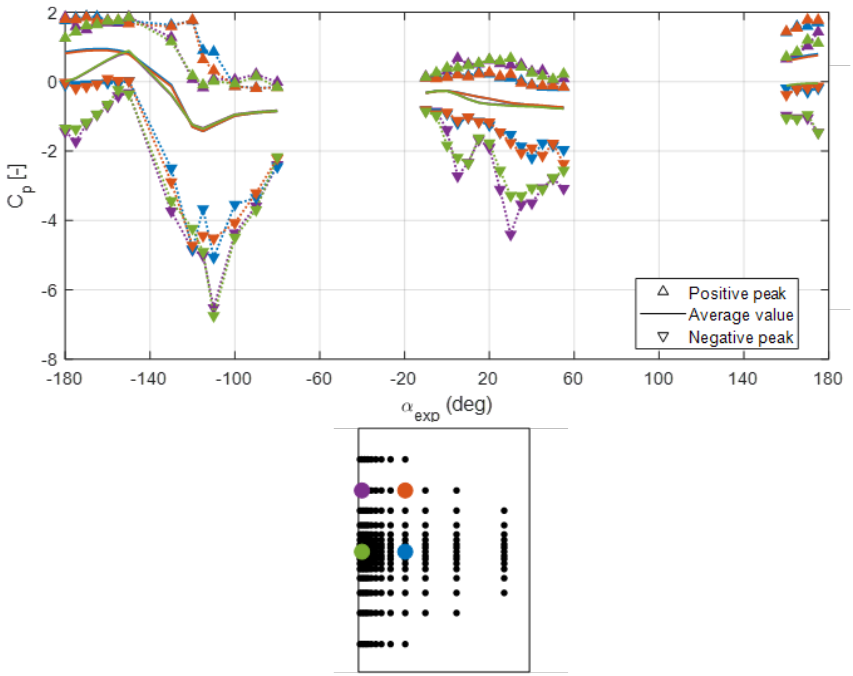

Figure 22: *Polar curve of average and expected maxima value for four pressure taps on Tile D*

Chapter 3

Statistical study of the peaks

In this chapter, a statistical study of the relationship between the spatial distribution and temporal duration of the peak events will be performed. The main purpose of this analysis is to study if a linear relationship between the duration and the spatial size (hereafter *width*) of the peak events exists.

Due to the extremely unevenness in the peaks' shape, an unambiguous definition of "peak", such as a definition of peak's width and duration, is elusive. To the authors' knowledge, no definition of "duration" or "size" of a peak exists in literature. In section 3.1 a definition of "peak", "peak's width" and "peak's duration" is proposed.

Following these definitions, an algorithm was written to extract from each single time-history all the peak events. All these events have been used to create a database with about one million entries. Each time-history is characterized by the following parameters:

- surrounding configuration (Stand alone or secondary building position)
- wind direction
- tap position

Then, within each time-history, each peak is characterized by its own values that are:

- duration
- width
- maximum C_p value

In section 3.2, using these informations the cross correlation between duration and width for several pressure taps is studied. In section 3.3 the results

will be compared to the existing state-of-the-art assumptions (i.e. the TVL equation).

In the following sections all the definitions hereafter are given assuming the peak to be positive events, to agree with the usual definitions of extreme event (e.g. the ones adopted for the wind statistics analysis). Since the peak studied in this thesis are negative (i.e. suction) events, before the analysis the pressure time-history is multiplied by -1 to transform the suction peaks into positive events. All the plots in this and the other chapters are obtained adopting the usual sign convection for the pressure field, that is negative for suction and positive for compression.

3.1 Peak extraction technique and definitions

A peak is defined as any data sample in a time-history with a magnitude larger than the magnitude of the previous and following samples. A minimum peak distance (0.05s) and a minimum peak threshold (equal to three standard deviations over the mean value of C_p) has been used to remove the smallest events.

Figure 23 illustrates an example of this methodology applied to one peak.

3.1.1 Peak threshold value

For each peak, a threshold value has been defined. This is required to compute its duration and width. The peak threshold value is defined as follows:

$$C_{p,ref} = \bar{C}_p + k\left(\hat{C}_{p,i} - \bar{C}_p\right) \tag{9}$$

where $\bar{C}_p$ is the average C_p value across the whole time-history, $\hat{C}_{p,i}$ is the maximum value of the considered peak and k is a number between 0 and 1, hereinafter *peak height fraction*. The results displayed a poor dependency from k. This will be analysed in section 3.1.4.

In figure 23-a the green line represents the average C_p value ($\bar{C}_p$), the vertical red line represents ($\hat{C}_{p,i} - \bar{C}_p$) and the vertical light blue line represents the same value scaled by k. Lastly, the horizontal dashed light blue line represents $C_{p,ref}$.

3.1.2 Duration

The duration of a peak is defined as the interval of time for which $C_p(t) \leq C_{p,ref}$ for the observed tap. This is represented in figure 23-a by the horizontal

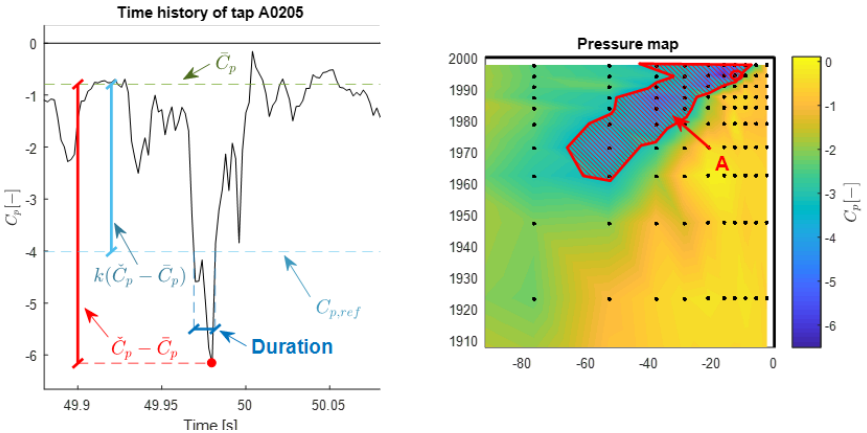

Figure 23: *Example of calculation of duration and width of a peak event. a) time history of the pressure measured in the tap indicated by the red circle with $C_{p,ref}$ and duration indicated. b) the surface of the building where $C_p \leq C_{p,ref}$. The width is equal to the square root of A*

dark blue line.

3.1.3 Width

The width of the peak is defined as the square root of the area of the tile that, the instant in which the peak occurs, is subject to a C_p value equal or higher than $C_{p,ref}$, i.e.:

$$w = \sqrt{A} = \sqrt{\iint_S f(x,y)dS} \tag{10}$$

with

$$f(x,y) = \begin{cases} 1 & C_p(x,y,\bar{t}) > C_{p,ref} \\ 0 & \text{elsewhere} \end{cases} \tag{11}$$

where S is the surface of the model, $C_{p,ref}$ is the peak threshold value and $\bar{t}$ is the instant at which the peak is occurring.

If two or more separated portions of the tile are subject to a pressure higher than the threshold value, only the patch containing the analysed probe is considered. Since in this research the pressure was measured simultaneously

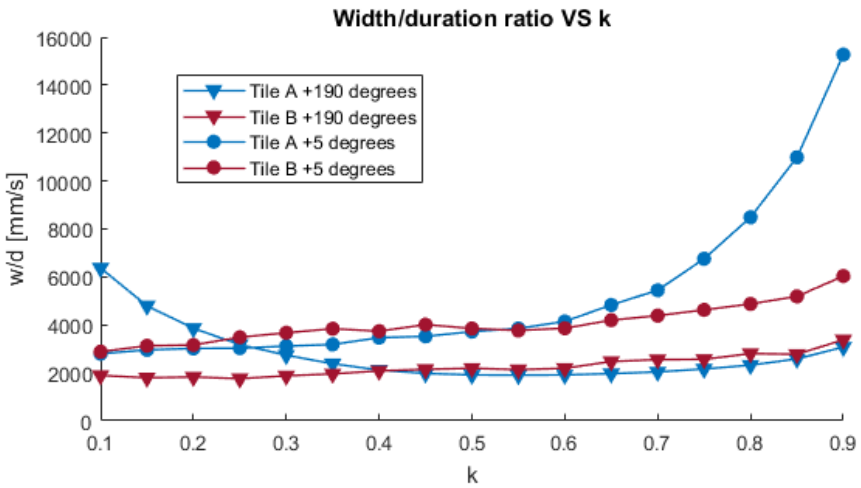

Figure 24: *Ratio of width over duration for different values of k for different taps*

only on a small portion of the surface and only on one face of the model, S is restricted to the analysed tile. In figure 23-b the instantaneous pressure field for $t = 49.98s$ is represented. The hatched portion represent the area where $C_p \geq C_{p,ref}$. The width is equal to the square root value of this area.

3.1.4 Dependency from the peak height fraction

The k parameter in the equation 9 represents the fraction of the peak "height" at which both the duration and the width are evaluated. A small value of k means that the duration of the peak is evaluated close to its “base”. This cause the value to be likely affected by the presence of neighbour noise in the signal that is not caused by the same physical mechanism that is causing the peak event. On the other hand, a value of k close to 1 means that the duration of the peak is evaluated close to its apex. This cause the duration to be small introducing more uncertainty due to the sampling frequency.

In 24 the average ratio between width and duration for a small set of taps and wind directions is shown. It appears that the ratio is acceptably constant for values of k between 0.3 and 0.7.

In 25 the Joint Probability Density Function (hereinafter JPDF) between the spatial width and the duration for two taps for different values of k are

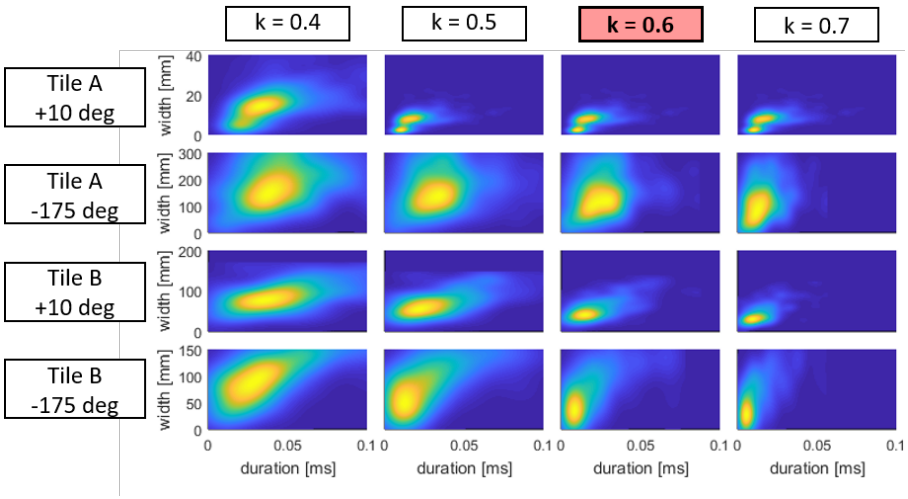

Figure 25: *Joint PDF for four taps for different values of k*

shown. A detailed description of these JPDF such as their meaning will be performed in section 3.2. For values of k between 0.5 and 0.7 the shape of the JPDF is almost not affected. The k value acts as a "scaling parameter", changing the scale of the JPDF, but not affecting much its shape. In this thesis, k was assumed equal to 0.6.

3.2 The duration-width correlation

As it was described before, the current state of the art adopts the hypothesis that the duration and the width of the pressure phenomena occurring on a model surface are linearly dependent. If this was the case, a simple low-pass filter in the time domain would eliminate from the time history the contribution of fast, and therefore concentrated, phenomena. Moreover, for this method to be applicable with a single cut-off frequency, the ratio between the duration and the width must remain constant all over the surface for all the exposures.

To test this hypothesis, for any given pressure tap and any given exposure all the peaks have been analysed with the method described in section 3.1. Depending on the tap, the number of peak analysed varies from about 150 to over 1500. For each peak, the width and the duration have been calculated.

After this, the JPDF between the duration and the width have been computed. If the previously mentioned hypothesis was verified, these JPDF should display a tendency to align on a diagonal line. The slope of this line would represent the proportionality factor between the width and the duration that would allow to compute the low-pass cut-off frequency given a certain spatial averaging area.

The survey will be conducted considering each wind direction, configuration and tap on his own. This choice allows to compare the relationship between the two parameters in different situations and understand if this is somehow constant or present some similarities.

Hereafter we will consider one by one some of the most significant cases, highlighting similarities and differences.

3.2.1 Top corner (tile A)

As can be seen from the extreme value polar curve in figure 17, for the top corner area two critical wind direction ranges can be identified. The first is the one for wind coming between 0 and 25 degrees, the second for wind coming between −180 and −135 degrees.

Hereafter two wind directions will be analysed, +10 degrees and −175, corresponding to the worst-case direction for each range.

In figure 26 the joint probability density function for 16 taps along 4 rows and 4 columns (indicated by the red arrows on the right) for $\alpha_{exp} = +10$ deg are presented. The taps in the top part of the tile (first two rows on Figure 12) present extremely concentrated peaks with low duration and width. The maximum of the JPDF for the top-row can be observed for durations equal to, respectively, 3.6, 3.6, 5.0 and 3.5 ms and for a width equal to 30, 20, 13 and 15 mm.

Observing the last row of figure 26 instead, representing the taps 236 mm below the first row, a completely different JPDF can be observed. In this case the mode of the distribution is located at d=10.8, 9.4, 14.4 and 9.4 ms and w=146, 209, 166 and 183 mm.

The ratio between the width and the duration of the most probable event for each tap can be interpreted as the equivalent convection velocity of the pressure field across the surface. If we compute this ratio, we obtain a value between 2.6 and 8.3 mm/ms for the first row and a value between 11.5 and 22.2 mm/ms for the last row.

The Pearson correlation coefficient is a measure of the linear correlation

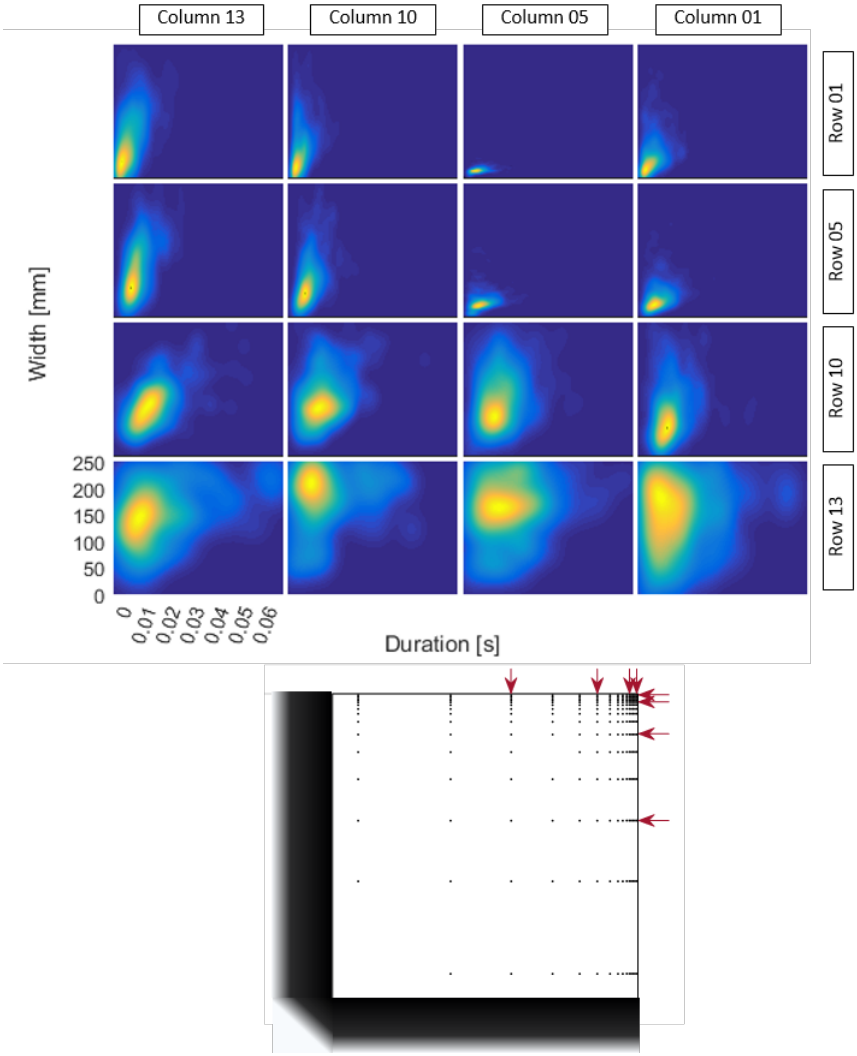

Figure 26: *JPDFs of duration versus width for the peaks recorded by several pressure taps on tile A. The top line of the plots represents the line of taps closer to the upper edge; the rightmost column represents the line of taps closer to the right-hand side of the tile. On the right, the arrows indicate the rows and the columns of the selected pressure taps; the black area represent the rest of the building. Test with exposure angle +10 degrees*

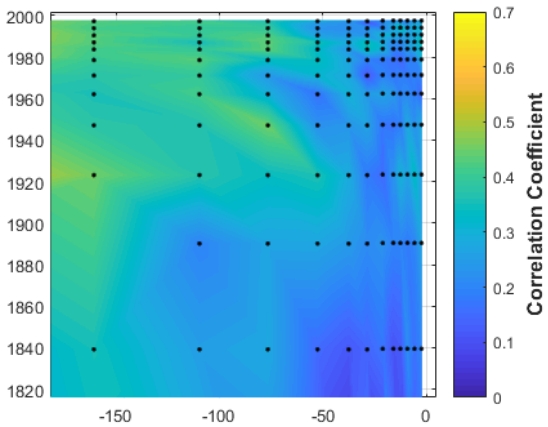

Figure 27: *Pearson correlation coefficient between peak duration and size for Tile A. Test with exposure angle +10 degrees*

between two variables X and Y and it is defined as:

$$\rho_{x,y} = \frac{\mathrm{cov}(x,y)}{\sigma_x \sigma_y} \tag{12}$$

where x and y are the two random variables; σ indicates the standard deviation and cov is the covariance. If applied to the values of duration and width, it gives an indication about how much the two parameters are linearly dependent.

The map of the correlation coefficient can be seen in figure 27. It can be observed how the correlation is lower than 0.5 everywhere and lower than 0.25 for a large portion (2.5m wide at full-scale) behind the leading edge. This suggests that in this area the assumption of linear proportionality between the duration and the size of the peak events could be wrong.

In figure 28 the JPDF between the width and the duration of the peak events measured in the same taps of Figure 26 for exposure -175 degrees is shown. These JPDF highlights the presence of slower and larger peaks. The JPDF of some taps (e.g. third and fourth columns) show almost a complete absence of correlation between the spatial size and temporal duration. This can be evinced by the almost-horizontal symmetry axis of the JPDF and is

confirmed by the low correlation coefficient in Figure 29.

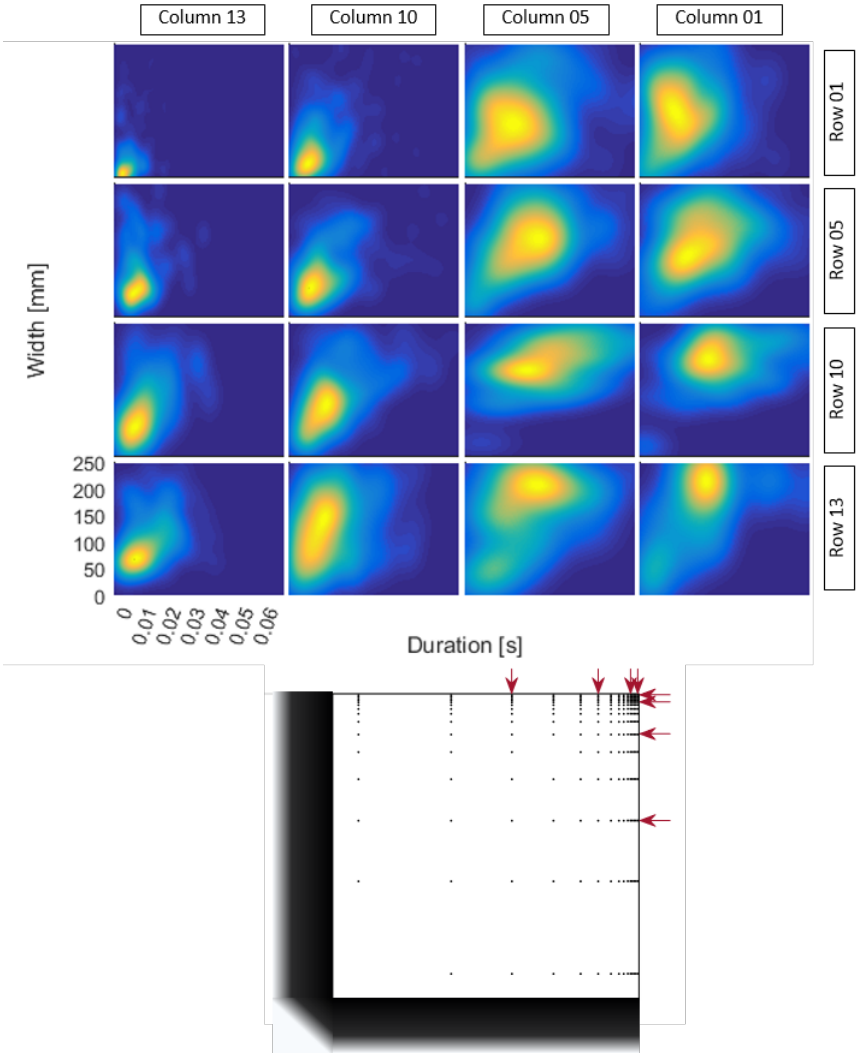

Figure 28: *JPDFs of duration versus width for the peaks recorded by several pressure taps on tile A. The top line of the plots represents the line of taps closer to the upper edge; the rightmost column represents the line of taps closer to the right-hand side of the tile. On the right, the arrows indicate the rows and the columns of the selected pressure taps; the black area represent the rest of the building. Test with exposure angle* -175 *degrees*

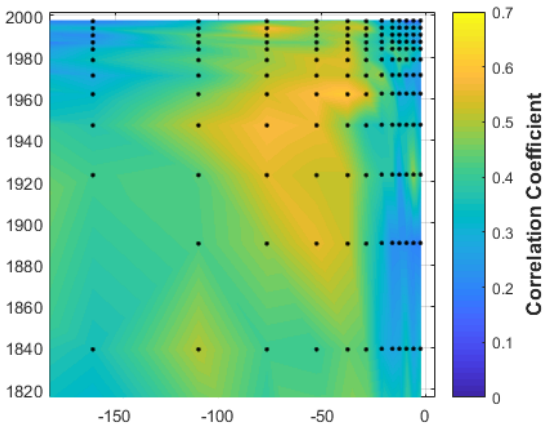

Figure 29: *Pearson correlation coefficient between peak duration and size for Tile A. Test with exposure angle −175 degrees*

3.2.2 Mid-height edge (tile B)

In the next paragraph we will repeat the same analysis performed in section 3.2.1 on the mid-height tile. As seen in section 2.5, the dimensioning value for wind coming from directions between −180 and −135 degrees is 4 times lower than the same value for the top-corner area. Despite this the analysis will be performed on the same two wind direction that can still be considered the worst case for the two wind direction ranges.

Figure 30 shows the JPDF of peaks measured for wind direction equal to $\alpha_{exp} = +10$ deg. The main differences appear to be in the horizontal direction. Being the boundary conditions constants along the y axis, it seems reasonable for the JPDFs to be similar for the taps belonging to the same column. As it was for the top-corner tile, the JPDF is not constant over the tile. The average duration of the peaks does not change significantly between the second and third columns, remaining equal to about 10ms. The average width, however, changes from 110mm to 40mm. This, again, indicates how phenomena with similar duration can have extremely different width depending on the considered position.

Figure 31 shows the correlation coefficient for Tile B with $\alpha_{exp} = +10$ deg.

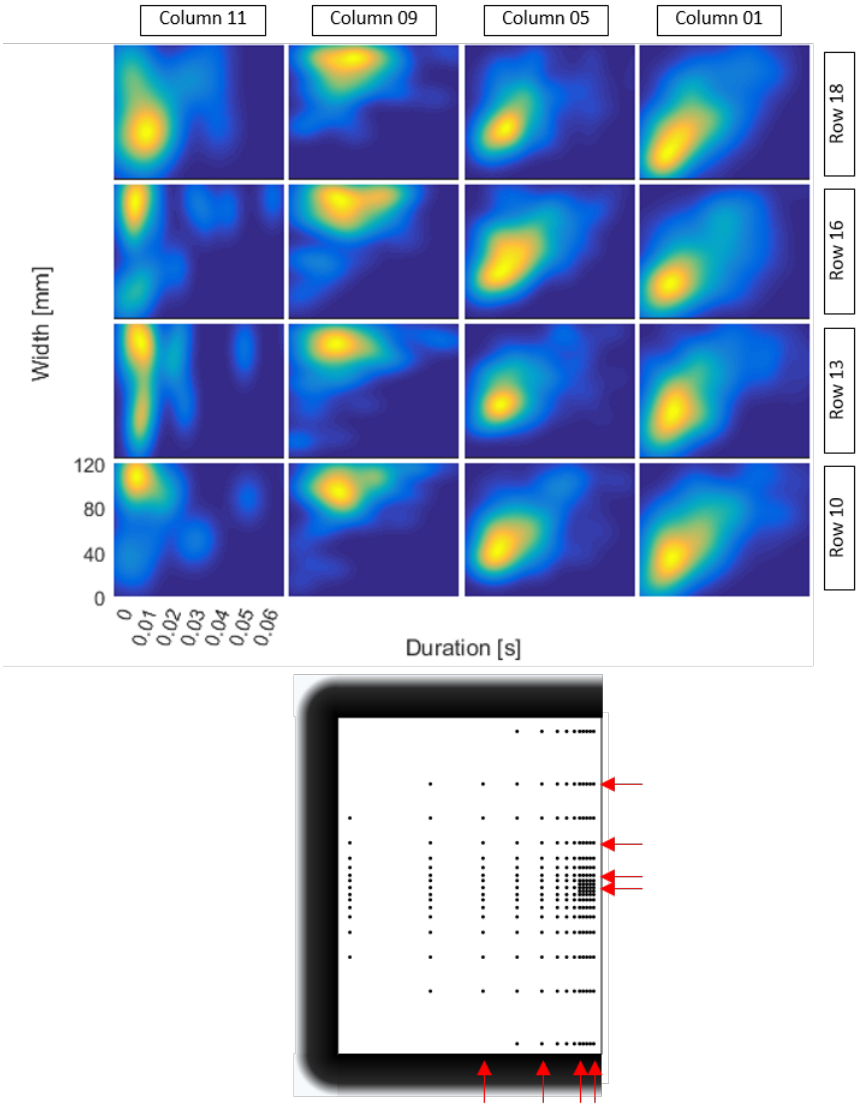

Figure 30: *JPDFs of duration versus width for the peaks recorded by several pressure taps on tile B. The bottom line of the plots represents the line of taps on the horizontal symmetry axis; the rightmost column represents the line of taps closer to the right-hand side of the tile. On the right, the arrows indicate the rows and the columns of the selected pressure taps; the black area represent the rest of the building. Test with exposure angle* -170 *degrees*

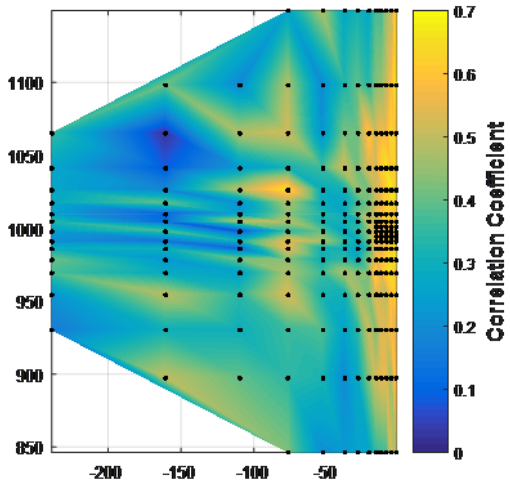

Figure 31: *Pearson correlation coefficient between peak duration and size for Tile B. Test with exposure angle +10 degrees*

In this case, the correlation coefficient close to the edge of the tile is equal to about 0.7 indicating a good grade of linear relationship between the duration and the width of the peak events.

Figure 32 shows the JPDF of peaks measured for wind direction equal to $\alpha_{exp} = +5deg$. As in figure 30, all the rows present similar patterns, indicating that the flow is bi dimensional as expected. The JPDFs of the taps behind the leading edge shows a distribution of the peaks that is almost "vertical". This means that, given a duration (being the most probable 0.01s) there is almost no information regarding the size of the peak.

Figure 33 shows the correlation coefficient for Tile B with $\alpha_{exp} = -175deg$. As in Figure 31, the correlation coefficient is again higher than 0.6 behind the leading edge of the tile, suggesting a good grade of linear relationship. This, however, is likely to be addressed to the vertical alignment of the JPDF of the taps behind the leading edge (Figure 32, rightmost column). As we have said before, this situation is not a symptom of the duration and the with being linearly dependent.

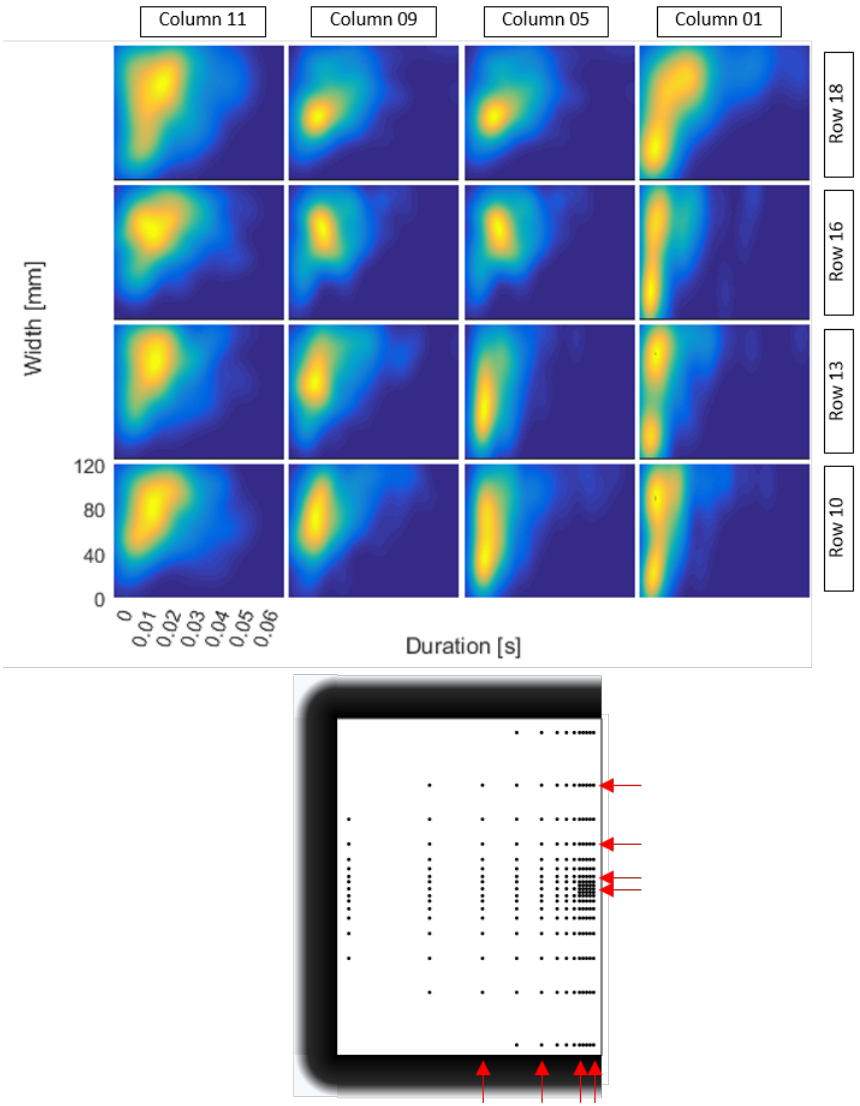

Figure 32: *JPDFs of duration versus width for the peaks recorded by several pressure taps on tile B. The bottom line of the plots represents the line of taps on the horizontal symmetry axis; the rightmost column represents the line of taps closer to the right-hand side of the tile. On the right, the arrows indicate the rows and the columns of the selected pressure taps; the black area represent the rest of the building. Test with exposure angle −175 degrees*

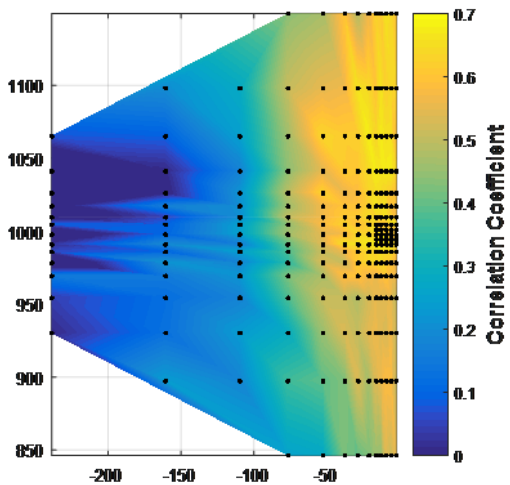

Figure 33: *Pearson correlation coefficient between peak duration and size for Tile B. Test with exposure angle −175 degrees*

Effect of an upstream building

Figure 34 shows the JPDF between the duration and the width of the peaks measured in the same 16 positions shown in figure 33 and with the same wind direction, but with the presence of an upwind building. This configuration was described in section 2.4.3.

If we compare this case with the stand-alone one, we can see that this time the phenomena occurring behind the leading edge of the building (rightmost column of figure 34) present strongly correlated duration and width.

A little farer from the leading edge, the peak events recorded presents a duration between 0.01 and 0.03 seconds, similar to the durations measured in the stand-alone case. In this situation however, the average width is about 50mm, about half the one measured in the stand-alone configuration. Another difference is the much smaller scatter of the data, with the standard deviation both of the duration and of the width that is about 2.4 times smaller than the same value in the stand-alone situation

3.3 The TVL parameter

In this section we will analyse the probability distribution of the ration between the duration and the width of each peak.

For each peak the ration between the duration and the width has been computed. This value, multiplied by the free stream velocity, corresponds to the parameter K present in the TVL equation

$$T = KL/V \qquad \Rightarrow \qquad K = VT/L \tag{13}$$

As we said in 1.1, based on full-scale measurements on Royex House in London, in the original TLV equation a value of 4.5 for K has been chosen as an appropriate one for the windward wall, when there are no other buildings upstream. In current usage the same value has been assumed for other building surfaces such as roofs and side walls. Holmes then suggested to change this value to 1, basing this assumption on the analytical integration of the admittance function over a typical cladding element dimension.

Figure 35 represents the PDF of the parameter K computed from five peak populations: black line is the PDF of the whole population of peaks extracted from all the taps, in all position, for all exposures in the present research; blue lines represent the PDF of the peaks occurring with $\alpha_{exp} = +10$; red lines represent the PDF of the peaks occurring with $\alpha_{exp} = -175$; dashed lines rep-

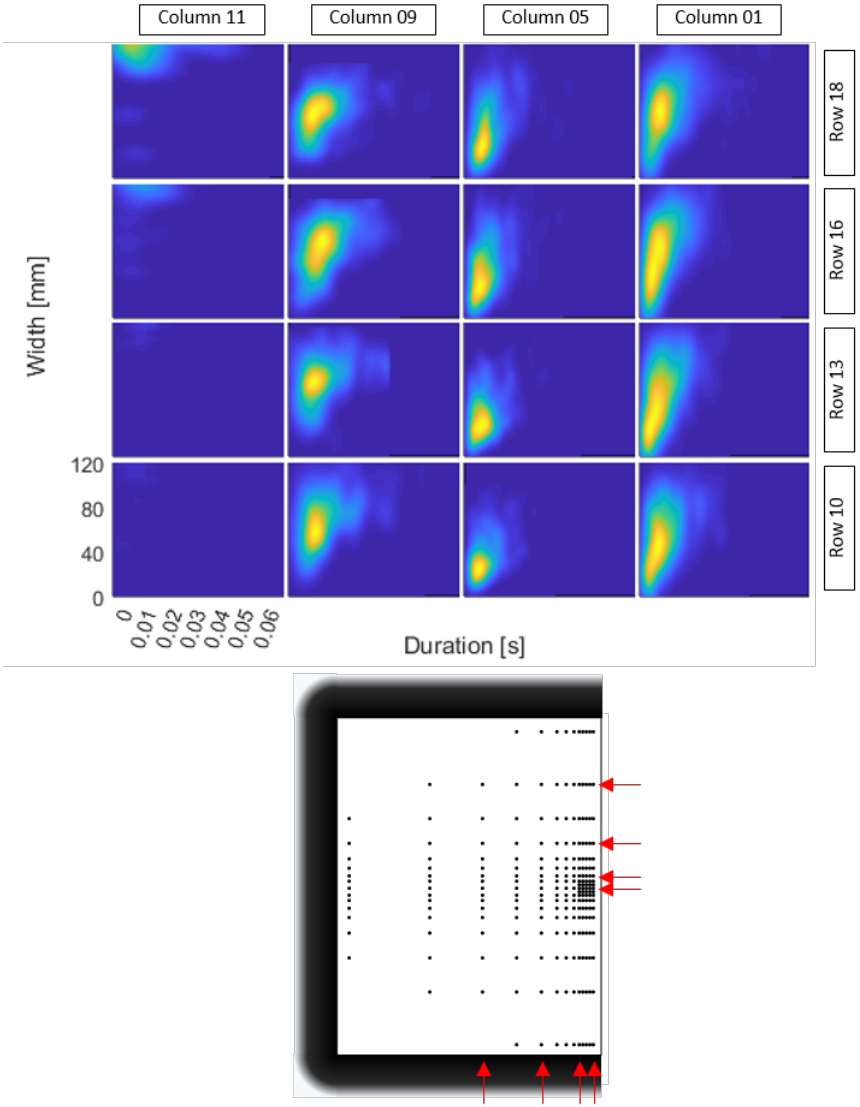

Figure 34: *JPDFs of duration versus width for the peaks recorded by several pressure taps on tile B. Test with exposure angle −175 degrees and the upwind secondary building in position "Pos2t"*

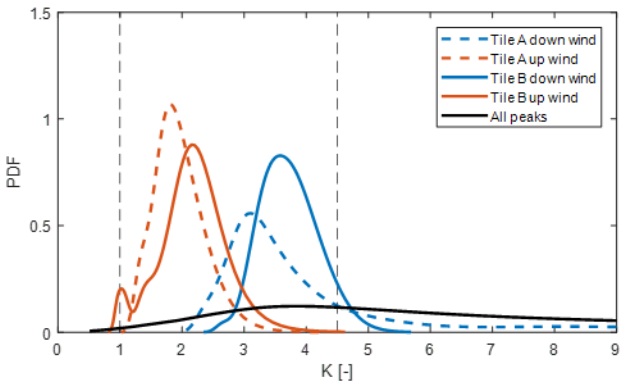

Figure 35: *Probability density function of the TVL's K parameter. The two vertical dashed lines indicates the values of 1 and 4.5 predicted, respectively, by Lawson and Holmes*

resent the PDF of the peaks occurring on Tile A; and continuous lines represent the PDF of the peaks occurring on Tile B. Observing the distributions, appears that the peak of the PDF computed from the whole population of peaks (about 600'000 events) is extremely close the value predicted by Lawson. However, this distribution is characterized by a large dispersion, with 51% of the events lying outside of the range $K = [2K_{Law}\ K_{Law}/2]$ with $K_{Law} = 4.5$. Looking at the PDF of the four individual cases, it can be seen how the mode of each distribution is far from 4.5, especially considering that for tile A the strongest (and therefore dimensioning) events occurs when in down-wind configuration, while for tile B occurs in up-wind configuration, that are the two PDF with the mode farer from the values prescribed by Lawson and Holmes. For these two PDF the modal value is equal, respectively, to $K = 3.1$ and $K = 2.1$.

In figure 36 are compared the two PDF of the K parameter for the peak measured for the wind coming from -175 degrees both with and without the upwind secondary building.

Both distributions are affected by a large dispersion with 50% of the peaks characterized by a value of K larger than 3.38 for the stand-alone case and 4.34 for the case with the secondary building. However, the main issue is that the modal value for the case with the secondary building is about 50% higher than the same value for the stand alone case. This result shows how different flow

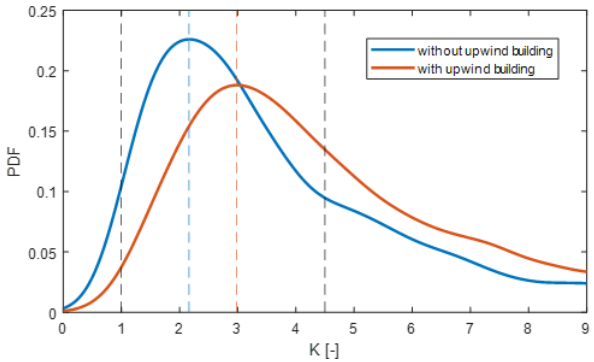

Figure 36: *Probability density function of the TVL's K parameter for the mid-height position with and without an upstream building. The two vertical dashed lines indicates the values of 1 and 4.5 predicted by Lawson and Holmes*

conditions, for example the presence of a shear layer of an upwind building, can severely affect the optimal value of K and, therefore, the cut-off frequency that should be used to post-process the data.

These results confirm (at least partially) the conclusions of Holmes that was predicting a K value equal to 1 for the windward face. It's important to remember that within this test campaign a real windward configuration, with the wind perpendicular to the instrumented area, hasn't been tested. Nonetheless, the value of K for $\alpha = -175$ degree is close to 1. For the tests with $\alpha = 10$ degrees, however, the value of K increases of about four times. This means that, for the same reference length L, a larger value of T - i.e. a lower cut-off frequency - need to be adopted.

These observations prove how a universal TVL equation, with a single universal K value, is probably too generic to hold true always and everywhere. Nonetheless, the smaller dispersions observed in the distributions of the K value for the single cases observed in figure 35 suggest that the TVL equation could be used if we were able to parametrize K as function of a series of variable taking into account the different flow situations on the different areas of the model. These variables could be, for example, the angle between the local normal to the surface and the wind direction, the distance from the leading edge, the presence of upwind obstacles, etc. This study hasn't been

done within the scope of this thesis, but is part of the ongoing work on the topic.

Chapter 4

Comparison with current state of the art

The final purpose of wind-tunnel tests is to asses the design loads to be provided to the façade designer. In the ideal case, the whole loading state of the cladding and the underneath support frame should be known. To achieve such level of detail, the whole pressure field distribution should be known. With the current state of the art, this is however impossible to be obtained with a wind tunnel experiment.

An intermediate solution between the complete knowledge of the pressure field distribution and the knowledge of the pressure in a single point is to assess the the average pressure acting on a cladding element.

As said in the previous chapters, the current state of the art tries to assess the average pressure field acting on an area equivalent to a cladding element taking into account its *analytical* spatial correlation. As we've seen, this translates in the above mentioned TLV equation.

In the experiment presented in chapter 2 we had a pressure taps spatial concentration high enough to be able to compute the *real* area-averaged pressure acting on some portions of the building surface. This allows us to compare the area-averaged value obtained experimentally with the time-averaged value obtained with the usual time-filtering techniques.

In this section we will try to understand which is the effect of the time-averaging and compare it with the *real* area-averaged value.

4.1 Methodology and motivation

The real nature of the wind induced pressure distribution on a building façade is represented by a pressure field varying with continuity both in time and

space. The mechanism that could lead to a cladding failure could be divided into two categories: the failures related to the glass panel and the failures related to the structural supports thereof.

The correct evaluation of the risk related to the first requires the integration of the load over time acting on the surface in order to evaluate the accumulation of damage in the glazed element (Calderone and Melbourne, 1993). A rigorous evaluation would also require taking into account the non-linearity of such damage accumulation, the initial tensile strength present in the element and the exposure to environmental factors. Since such technique is often impractical and too complex, manufacturers often produce simplified charts obtained from their own performed tests. It should be anyway pointed out as a very limited number of failures could be addressed to the breaking of the grazed element due to the bare force of the wind.

The latter and more common mechanism of failure is represented by the collapse of the supports of the panel. This can be in first instance assessed considering the instantaneous force acting of the cladding element. This research will focus on this latter failure mechanism and on the evaluation of the design load for the supports elements.

Thanks to the high pressure taps density used during the wind tunnel test, the total force acting on the surface element could be assessed by a discretized integral over a surface with the same full scale dimension of a typical cladding panel. Dividing then by the total element surface, the average pressure acting on the element is evaluated as:

$$p_{AA}(t) = \frac{\sum p_i(t) A_i}{A_{tot}} \tag{14}$$

where p_{AA} is the area-averaged pressure on the panel; p_i is the pressure recorded by the i-th tap, A_i is the intersection between the influence area of the i-th tap and the surface of the panel and A_{tot} is the total area of the panel (i.e. $A_{tot} = \sum A_i$). Worth noting that having been filtered only in the space domain and not in the time domain, the resulting time-history is characterized by a continuum spectrum from 0 to the Nyquist frequency of the sampling system.

The obtained signal can then be analysed using the usual extreme events evaluating techniques, such as (Cook& Mayne, Gumbel, Harris' XIMIS, ecc). An overview of several methods for the estimation of peak wind loads can be found in (Peng et al., 2014).

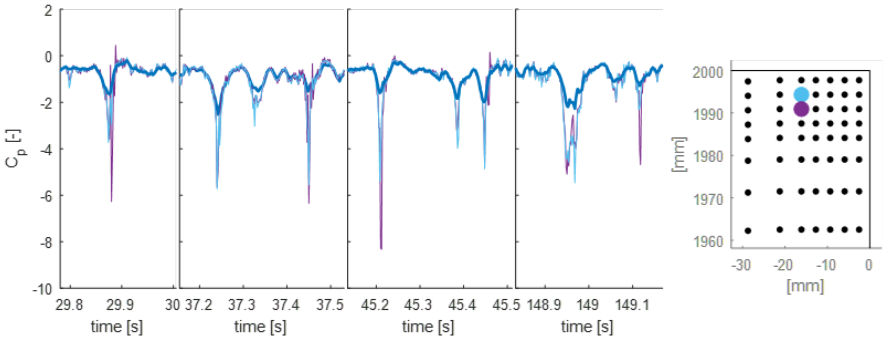

Figure 37: *Comparison between the signal of two pressure taps on tile A and the area-averaged value on a 2m by 3m panel. The colours correspond to the two taps indicated on the map on the right.*

4.2 Single signal comparison

Figure 37 shows the comparison between some "pieces" of the signals of two pressure taps of the top-corner tile and the area averaged signal on a surface equivalent to a 2m by 3m panel in the same area. The area averaged signal is obtained averaging the signals of 72 different pressure taps (two of which are the ones shown). Figure 38 shows a similar comparison performed for the mid-height tile.

The figures show how the area average applied to the signal recorded on the top corner of the building causes a severe reduction of most of the peaks observed in the signal of the single taps, while the reduction is considerably lower in the case of the mid-height tile.

What is even more important is to point out that the ratio between the minima reached by the single-tap time-histories and the minima of the area-averaged time-history is very different for the two tiles, but also for similar peaks occurring in the same tile. For tile A, in the second window, two peak events are present. The first event reached a peak value of $-5.7C_p$, while the second reached a peak value of $-6.35C_p$. Once averaged over the 2m by 3m area, the first is reduced to $-2.5C_p$, that is a 56% reduction, while the second is reduced to $-1.5C_p$, that is a 75% reduction.

Looking at the second and third window in figure 38 we can see two peak events, both with a duration of approximately $0.1s$. However, while for the

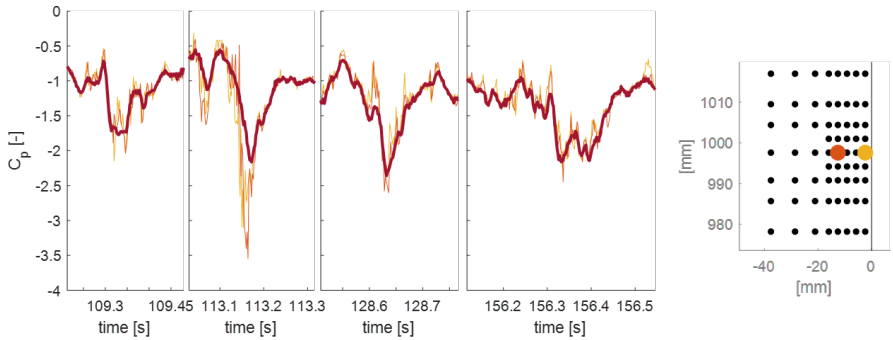

Figure 38: *Comparison between the signal of two pressure taps on tile B and the area-averaged value on a 2m by 3m panel. The colours correspond to the two taps indicated on the map on the right.*

first the peak area-averaged value is about half the peak single-tap value, for the second the reduction is almost negligible.

These considerations can be quantitatively evaluated from figure 39. Here are represented the PDFs of the difference between the peaks evaluated in the signal of a single tap and the same ones evaluated in the area averaged signal.

It is clear that for the case of taps on tile A (top-corner) the reduction can be estimated in the order of $-2C_p$, while for taps on tile B the reduction is often negligible.

Figure 40 shows the spectra of the signal presented in figure 37 and 38. The lower x-axis represent the non-dimensionalized frequency, while the upper x-axis represent the corresponding full-scale frequency (for $\bar{U}_{50m} = 28$m/s and $\lambda_L = 1:50$). Two main differences arise:

- the pressure signals of Tile A have the energy peak shifted towards higher frequencies ($\approx$ 0.6Hz full scale) highlighting the presence of the faster phenomena seen in figure 37
- the energy reduction for Tile B due to the area averaging is only significant for fB/U_{ref} higher than $1 \div 3$ – i.e. a full-scale frequency of 0.55Hz, while for Tile A the reduction is significant also for lower frequencies with a reduction of the energy density in the order of $5 \div 10$ times.

Even if this comparison took into consideration the signals of only few taps in two particular tests, it highlights the fact that the effect of the area averaging

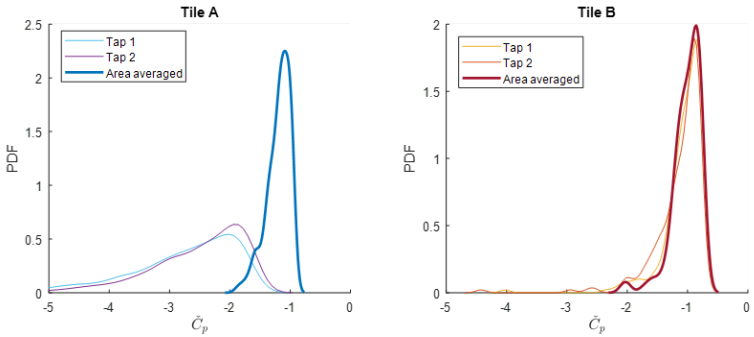

Figure 39: *Probability density functions of the peak values of the 6 time-histories in figure 37 and 38. The colours corresponds to the position showed in the two previous figures*

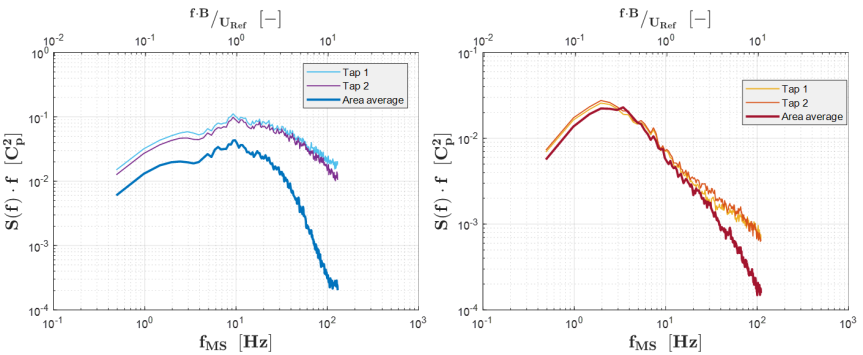

Figure 40: *Spectra of the 6 time-histories in figure 37 and 38. The colours corresponds to the position showed in the two previous figures*

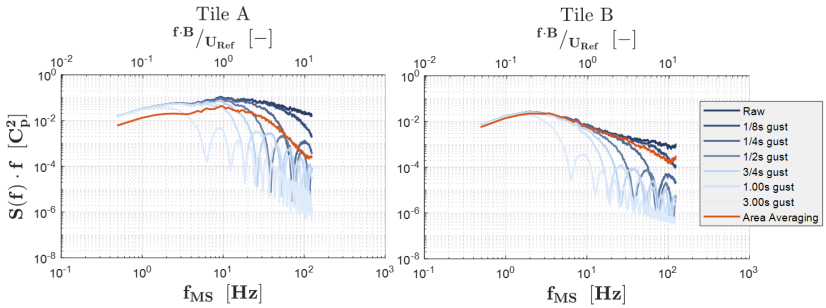

Figure 41: *Comparison between the spectra of two raw time-histories in figure 37 and 38, the spectra of the same time-histories filtered in the time domain and the spectrum of the area-averaged time-history.*

technique is strongly influenced by the position of the tap.

In the author's opinion, this is due to the fact that the pressure signals measured by a single tap contain the contribution of different types of phenomena whose importance depend on the position of the point analysed (as well as other external factors, such as the turbulence caused by a second upwind body, as we'll show later on). This is in agreement with the findings of chapter 3. The impact that the area averaging technique has on these phenomena is different for each of them, causing the overall effect of the area averaging to change from point to point.

Figure 41 shows the comparison between the spectrum of the area averaged signal and the time averaged ones. For the mid-height tile (Figure 41 right) a low-pass filter with a cut-off period of 0.5s can reproduce the behaviour of the area-averaging satisfactorily. For the top-corner tile instead no time filter can effectively reproduce the spectrum of the area averaged sigma, since no low-pass time-filter can catch the reduction in the low frequency range without severely affecting the peak at $fB/U = 1$.

The ripples of the time averaged spectra could be drastically reduced using a better low pass filter. In this research the moving average has been used to be consist with the current practice. The conclusions are not affected by this choice.

4.3 Effect on the design value

In the previous section we analysed in detail the behaviour of the time filtering and the area filtering on a small sub-set of signals. In the next section we will compare their behaviour looking at the design value that are obtained in the various part of the building using different moving-average spans.

To do so, each time history has been analysed with the Cook and Mayne procedure to extract the expected minimum value for each wind direction. Taking the lowest value among all the wind directions for each tap produced the envelope of the negative peak pressure. This envelope is the one associated with the *raw* signals (Yellow box in figure 42).

This procedure has been repeated filtering each time history with a moving average filter prior to the Cook and Mayne procedure. Doing this, an envelope for each span of the moving average filter has been produced (Red box in figure 42).

A last envelope has been produced dividing the model surface in rectangular areas with the dimensions of a typical cladding panel. For each portion of surface, then, the area average time history has been calculated using equation eq:areaAverage. These area-averaged time histories have been then analysed too with the Cook and Mayne procedure to produce the envelope of the negative peak area-averaged pressure (Light blue box in figure 42).

Since the value against which we want to make the comparison is the area-averaged pressure, this last envelope has been assumed as the reference one. All the other envelopes have been then analysed in terms of **difference with respect to the envelope obtained with the area-averaged pressure** (Green box in figure 42).

4.3.1 Some considerations on the comparison method

The comparison of the pressure maps is done in terms of difference of expected minimum C_p ($\Delta\check{C}_p$). It is indeed important to remember that all the pressure coefficients that are computed in any cladding test are referred to an arbitrary reference pressure. The definition of such pressure involves usually the gradient pressure or the roof height free stream static pressure. Whichever the definition of such pressure is – which changes wind tunnel to wind tunnel – the value itself is of no interest for the cladding design. The overall force acting on a panel is indeed the difference of two pressures: the external one, computed during the wind tunnel tests, and the internal one.

The value of the latter is a largely debated topic and a univocal definition does not exists. For building with no active pressurization, this could be

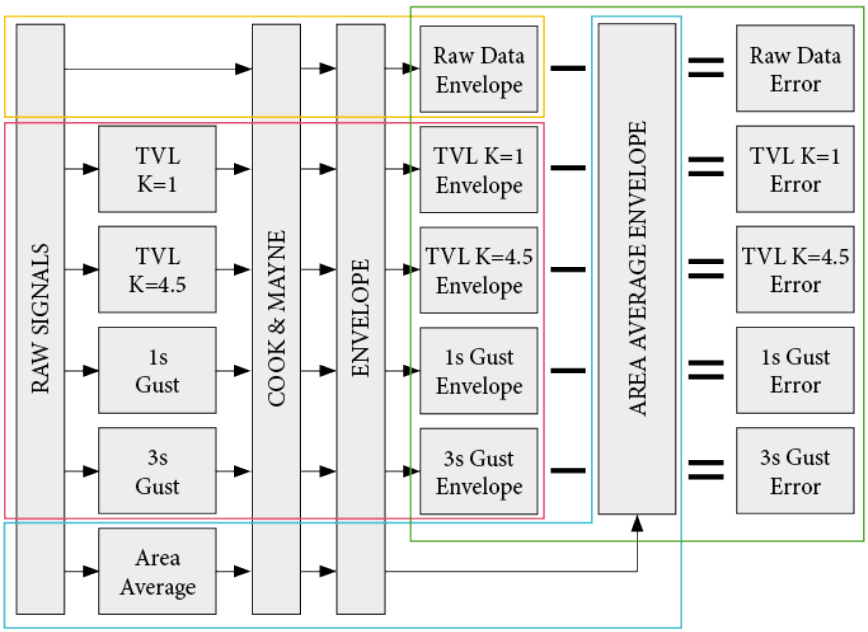

Figure 42: *Schematic view of the procedure used to produce the error maps*

assumed - in first instance - as the average pressure acting on the external surface, assuming a homogeneous porosity distributed across the building surface. If a ventilation system exists, the internal pressure could be actively controlled or assumed to be related to the pressure at the ventilating system's inlet. Lastly, if the building has one or more prevailing openings, the internal pressure should be computed as a weighted average of the pressure on each

opening plus a contribution - often negligible - of the overall pressure on the building's cladding.

In any of those case, however, the values of the cladding pressures obtained in wind tunnel testing should be assumed up to an additive constant. This observation lead to the impossibility of comparing to pressure fields as ratio of one over the other. Such ratio indeed would be function of the above mentioned additive constant who depends by building characteristics that lie outside of a wind tunnel cladding test scope.

For this reason, the following maps will represent a difference (rather than a ratio).

4.3.2 Dependency from the position on the building

Figure 43 shows the Cp difference between the negative envelope computed using the data averaged over a 2m by 3m area and the ones computed with the data filtered with a moving-average filter in the time domain with different span. For such area, the TVL equation suggests to use a time span τ equal to 0.12 seconds if one assumes $K = 1$ (Holmes version) or $\tau = 0.54$ seconds assuming $K = 4.5$ (Lawson version). Two other values for the time-average are tested: the *1 second gust* and the *3 sec gust*.

In the plots, the blue areas are those where the area average is predicting a less negative value – i.e. use of the time filtering lead to an over-estimation of the design load in that position; vice versa the red areas are those where the area average is predicting a more negative value – i.e. use of the time filtering lead to an under-estimation of the design load.

The red rectangle represents the dimension of a 2m-by-3m panel and it's used as reference. The rectangle also indicates the position of the tile where the taps are more concentrated. The black lines indicate the edges of the building.

It is clear that the pressures analysed without applying any filter lead to severely overestimated values. In some regions – e.g. the top corner – the design value obtained from the raw data is more than 2 C_p lower than the area-average one.

On the other hand, the 3 second gust is severely underestimating the pressure with an average error in the order of $1.5 \div 2C_p$.

The TVL using $K = 1$ tends to overestimate the design value. This is most critical close to the top corner and close to the leading edge of the building. In these areas the underestimation can be higher than $1C_p$.

In this comparison, the best choice seems to be the value predicted by the

TVL equation with $K = 4.5$. Using the duration predicted by the Lawson equation leads to design value that are less than $1C_p$ off of the area-averaged value in almost every point. Only in a small area close the the top corner the design value predicted by using the TVL equation are more than $1C_p$ apart from the one obtained using the area-averaged time-histories. This is in agreement with the finding of section 3.3.

4.3.3 Dependency from the cladding size

In figures 44 and 45 the design value predicted using the area-averaged time-histories is compared to the value obtained using the time-averaged data for different averaging sizes. The first row of the two figures represent the error when a $1.5m \times 1.5m$ area is considered, the second row is again the typical $2m \times 3m$ cladding size and the third row represents a $5m \times 5m$ averaging area.

This time, since the span of the moving average predicted by TVL equation is proportional to the diagonal length, the values of τ for the second and the third columns is different on each row. These values are summarized in table 1. The first, fourth and fifth columns represents again the error performed using, respectively, no filter, 1 second moving average and 3 second moving average.

For the area close to the top corner of the building, the TLV equation with $K = 1$ tends to overestimate the design value of about $0.5C_p$ almost everywhere, with the worst situation occurring close to the corner, with an overestimation that is sometimes larger than $3C_p$. The situation when using the TVL-prescribed span with $K = 4.5$ is about the opposite, with an overall underestimation of the design load that, close to the corner, can be in the order of $1C_p$. It is interesting to see that the taps positioned in the small triangular critical area close to the corner tends to *overestimate* the design value even when using $K = 4.5$!

The behaviour of the 1 second gust and the 3 second gust is strongly dependent, as expected, from the cladding size. Generally speaking, they both tend to underestimate the design value, with the worst situation occurring when using the 3 second gust with a small tiling.

For the area at mid-height (tile B) the situation is less critical. It can be seen that, again, the designed values obtain with the TVL using $K = 1$ tends to be slightly overestimated, but never exceeds $1C_p$ difference to the area-averaged value. On the other hand, the values obtained using $K = 4.5$ tends to be just slightly overestimated and are everywhere between 0 and $0.5C_p$ lower than the area-averaged values.

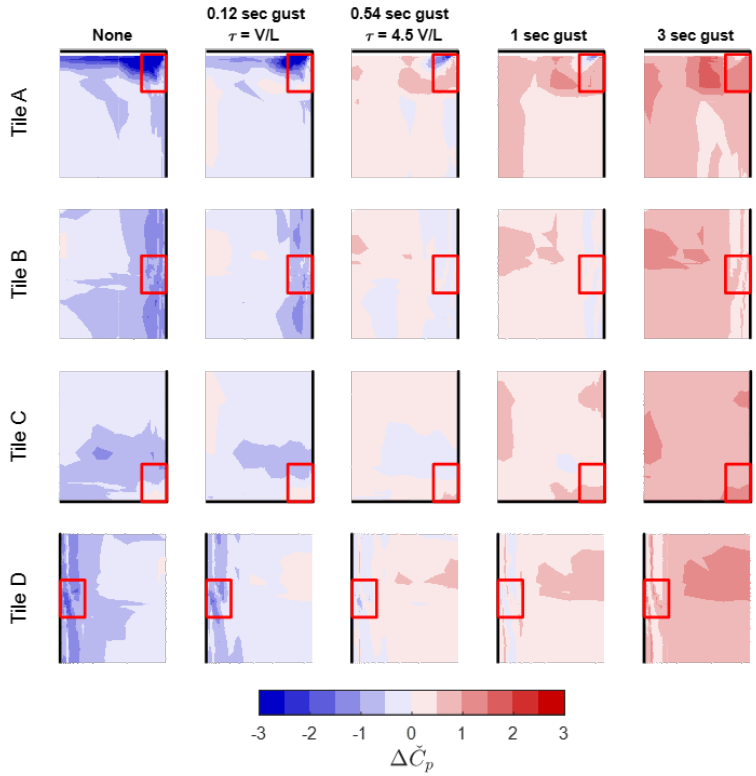

Figure 43: *Error comparison on the evaluation of the negative peak envelope with respect to the area average. Red indicates areas where the time-averaging is underestimating the design load. Blue areas correspond to areas where the time-averaging is overestimating the design load*

Panel size	$\tau = L/V$	$\tau = 4.5L/V$
$1.5m \times 1.5m$	0.074 s	0.335 s
$2m \times 3m$	0.120 s	0.540 s
$5m \times 5m$	0.248 s	1.116 s

Table 1: *Spans of the time-average used for figure 44*

Again, the error performed using the 1 or 3 second gust is function of the averaging are they are compared to, but they both tend to underestimate the design load.

4.3.4 Effect of an upwind building

The value of K in the original TVL equation has been chosen as an appropriate one for where there are no other buildings upstream (Lawson, 1976). In many urban environment however, this is not the case. It is a consolidated practice in wind-tunnel, indeed, to physically reproduce no only the tested building, but also the surrounding structures.

However, since no correction for the TVL equation exists when there are other buildings upstream, the original formulation is extended to these situations.

To evaluate the effect of an upstream obstacle on the façade design value, the wind tunnel tests has been repeated placing a lower building close to the tested one. The distance between the two building was chosen to be equal to 400 millimetres, that, considering a geometric scale equal to 1:50, correspond to 20 metres, that is the width of an average road. The height of the building has been tuned in order to achieve the lowest design peak value exactly at 1000 mm from the ground, that was the area with the higher taps density. A sketch of the tested configuration can be seen in figure 46.

Figure 47 shows the comparison of the design value with time and area filtering when the second building is present. Comparing this with figure 45, we can see that the error performed using the TVL equation with $K = 1$ is much higher than the stand-alone case.

The most critical zone is the first column of panels just behind the leading edge. For a small cladding size ($1.5m \times 1.5m$) the error is between -1 and

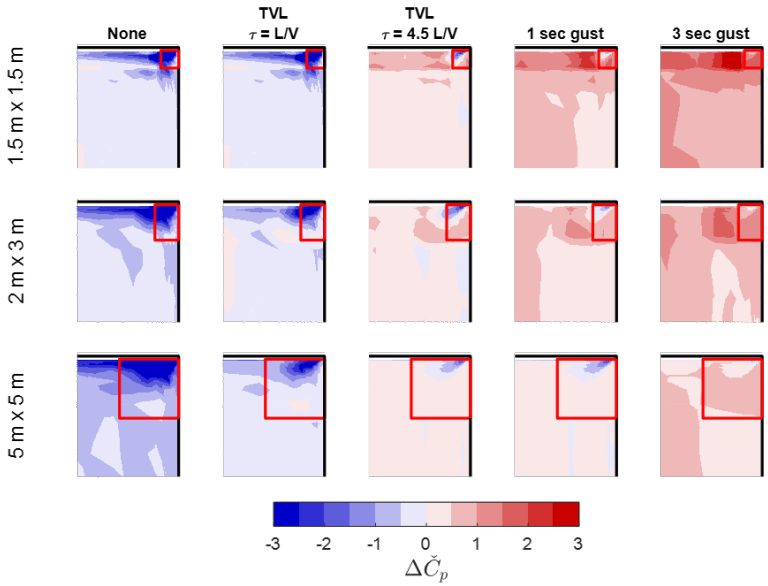

Figure 44: *Error comparison on the evaluation of the negative peak envelope with respect to the area average as function of the averaging area on Tile A*

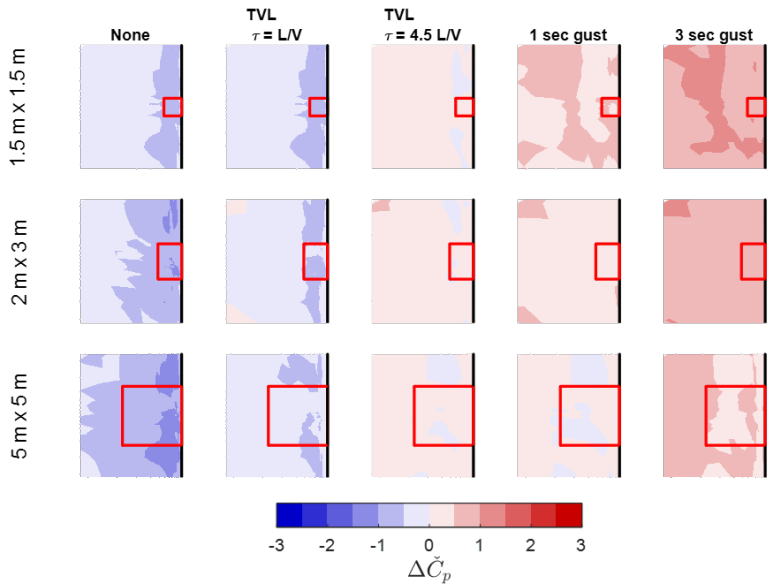

Figure 45: *Error comparison on the evaluation of the negative peak envelope with respect to the area average as function of the averaging area on Tile B*

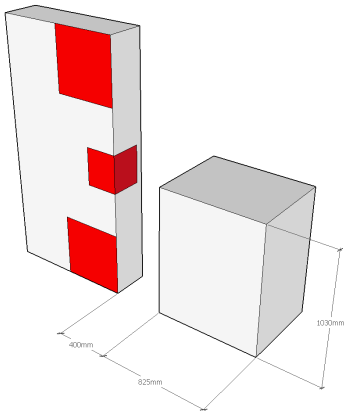

Figure 46: *Configuration used to test the influence of an upstream building*

$-3C_p$. The situation is slightly better for larger panels where the error drops in the range -1 to $-2C_p$.

On the contrary, the error performed using the TVL equation in the original Lawson form leads to error that are not much different from the stand-alone case i.e. an error of less than $\pm 0.5C_p$.

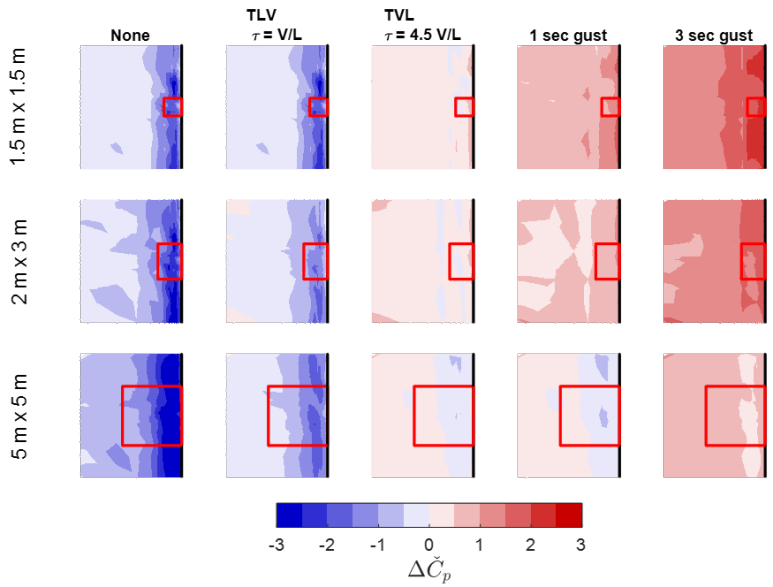

Figure 47: *Error comparison on the evaluation of the negative peak envelope with respect to the area average as function of the averaging area on Tile B with an upwind building*

Chapter 5

The smart pressure tap

In the previous chapter we studied the outcome of the experimental high-resolution space-time survey of the pressure distribution in some critical areas of a building surface.

Chapter 3 highlighted how the assumption that the duration of *any* pressure fluctuation is proportional to its spatial width is, in general, false. In particular, we saw that the proportionality factor between the spatial and temporal size of the pressure fluctuations, when it exists, changes from point to point and exposure to exposure.

The result seems to lead to the direction that a *single* cut-off frequency that could be used to filter all the pressure data of a whole experimental campaign to remove the events smaller than a certain threshold could not be found.

In chapter 4, however, we found that taking a cut-off frequency evaluated using the original Lawson's TVL equation led to a dimensioning value that is almost everywhere less than $1C_p$ off from the design value evaluated using an the area-averaged time-histories.

Nonetheless three main problem arise:

- In some areas (e.g. the top corner of the tested building) the error is far from being negligible when using the TVL-prescribed time-filter. This can be seen in figure 48 where a zoom in the top corner shows how the error can exceed 3 C_p.
  For simple geometries, such as the one tested in this campaign, it could be rather simple to draw up a list of the "critical" position where the results of single-tap measurement cannot be considered reliable. However, it is almost impossible to know which are these position when testing complex geometries for which the pressure field is *a priori* unknown, that are,

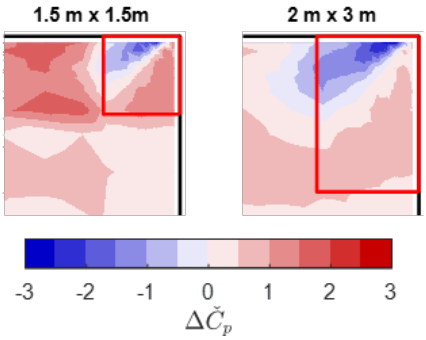

Figure 48: *Error comparison close to the building's corner on the evaluation of the negative peak envelope with respect to the area average when filtering the data using the Lawson TVL time-filter*

indeed, the main reason why wind tunnel testing are performed.

– In order to achieve a more precise evaluation of the pressure effect on the cladding, we should multiply the spectrum of the overall force acting on the cladding by the Frequency Response Function of the cladding system.
  However, as we have seen in figure 41, the spectrum of the time-averaged signal is completely different from the spectrum of the area-averaged one. For this reason, any effect of the FRF of the supporting system cannot be taken into account.
– Another way to improve the evaluation of the pressure effect of the cladding support system would be, as already pointed out by Holmes (1997), to take into account the influence surface for the *effect* we are interested in (e.g. reactions, bending moments, stresses, etc.). To do so with single-tap data is virtually impossible.

These issues, especially the last two, cannot be solved using the current single-point testing methodology.

Historically, unsteady spatially-averaged loads have been measured either by using special purpose transducer (such as force balances of diaphragm pressure transducers) or through the numerical average of a discrete number of pressure taps. Both these approaches however, present intrinsic difficulties. The former is relatively inflexible and introduces the loading function (i.e. the influence

surface) of the diaphragm into the response of the system. The latter corresponds exactly to what has been done in the research presented in this thesis. This, while extremely flexible and accurate, is also extremely expensive. At the moment of writing, the average price for a pressure measurement channel is equal to about 1000 euros. For this reason, extending the approach used in this thesis to a whole model would be unfeasible.

In order to overcome these problems and achieve a more reliable measure, a new experimental approach has been developed. This is especially focused to the **direct measurement of the area-averaged pressure acting on an area with an arbitrary size and shape**.

A similar attempt to use a pneumatic averaging technique to solve the area-averaging problem was firstly proposed by Surry and Stathopoulos in (Surry and Stathopoulos, 1978). Their solution was to connect a certain number of pressure taps (2 or 8) to a single manifold. The pressure in the manifold was then acquired using a traditional pressure scanning system. The technique presented in this work can be considered as an extension of the Surry and Stathopoulos work, but with a simpler and more efficient design. It, indeed, removes the need of a large number of tubing systems connecting to several central manifolds.

The new device/approach should then provide a number of characteristics:

- to be able to correctly measure the area-averaged pressure;
- to be easy to be installed;
- to be as cheap as possible and
- to be as compatible as possible to current experimental techniques and equipment

The solution chosen, hereafter called *AZA tap*, has been to use a porous panel with the prescribed size and shape in front of a small cavity within which the pressure is measured with a usual pressure tap. A 3D sketch of the tested device can be seen in figure 49.

5.1 Analytical formulation

Assuming the flow through the porous surface to be small, the pressure inside an opening with multiple openings can be assumed to be equal to:

$$p_{AZA} = \frac{\sum p_i A_i}{\sum A_i} \tag{15}$$

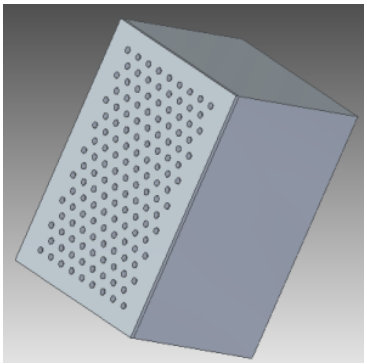

Figure 49: *A three dimensional sketch of the proposed measurement device*

where p_i is the pressure acting on the i-th opening and A_i is the cross-section of the i-th opening. Assuming all the holes to have the same dimension and to be evenly distributed across the surface, the pressure inside the measurement box can be - in first instance - assumed to be equal to the average pressure acting on the outer face of the porous panel.

Some problems could arise if the resonance frequencies of the cavity fall within the measurement's frequency range. For a closed cavity with a porous panel, two categories of resonance can be identified.

The firsts are the acoustic modes of the cavity. For a rectangular box the first resonance frequency is equal to:

$$f_1 = \frac{c}{2} \frac{1}{\max(L_x, L_y, L_z)} \tag{16}$$

where c is the speed of sound and $L_{x,y,z}$ are the dimensions of the box. Assuming the speed of sound to be equal to 343 metres per second and a maximum dimension of 100 millimetres (corresponding to a 5m panel in 1:50 scale), the first resonance frequency is equal to about 3500Hz.

The second family of resonance modes are the ones related to the Helmholtz frequency. For a single-hole cavity, the Helmholtz frequency is equal to

$$f_H = \frac{c}{2\pi} \sqrt{\frac{A_\phi}{V_0(L + \delta_{tot})}} \tag{17}$$

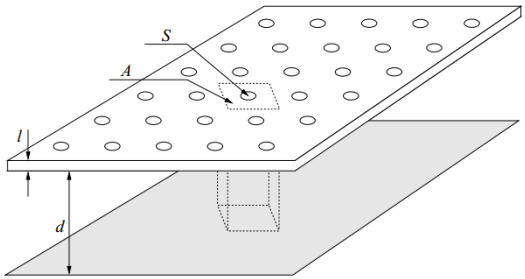

Figure 50: *A perforated panel. This is an example of distributed Helmholtz resonators. Each panel opening with cross-section area S has an associated cavity volume $A_\phi d$. The resonator neck length l equals the thickness of the panel (From (Randeberg, 2000)*

where A_ϕ is the cross section of the hole, V_0 is the volume of the cavity , L is the length of the neck and δ_{tot} is a correction factor to take into account the end losses.

An infinitely wide porous surface in front of a flat plate can be modelled as a distributed Helmholtz resonator (figure 50). In this case the resonance frequency can be written as (Randeberg, 2000):

$$f_H = \frac{c}{2\pi}\sqrt{\frac{\phi}{d(l+\delta_{tot})}} \tag{18}$$

where ϕ is the panel porosity, defined as the ratio between the total area of the openings and the area of the panel, d is the distance between the porous panel and the back plate, l is the panel thickness and δ_{tot} is a correction to the neck length that is equal to:

$$\delta_{tot} = \frac{16r}{3\pi} \tag{19}$$

where r is the radius of the holes.

In our case, assuming a porosity equal to 30%, a distance d equal to 40mm, a panel thickness equal to 1mm and a hole radius equal to 1mm, leads to a resonance frequency equal to 2878Hz.

Both resonance frequencies are therefore well beyond the normal measurement frequency range that usually goes from 0 to 500Hz. The volume of air inside the box will therefore work in a quasi-static frequency range, avoiding any resonance phenomenon.

To confirm these conclusions, the frequency response of the device has been tested experimentally using a flat wave generator. The frequency response has been proven to be virtually flat (and with zero lag) in the frequency range from 0 to 250Hz.

5.2 Experimental set up

Figure 51 shows the tested device mounted on the model. The tested device was made of a 40mm by 60mm PMMA (Plexiglass) panel mounted on top of a 40 by 40 by 60 foam box. On the front panel a staggered array of holes with a diameter equal to 2mm has been cut using a laser-cutting machinery. The distance of the holes has been taken equal to 3.5mm in order to achieve a porosity equal to 30% of the total area.

A second panel with a porosity equal to 10% and a hole diameter equal to 0.5mm has been tested.

Both tested devices were instrumented with two pressure taps on the back of the device and two pressure taps on the outside of the porous panel. A section of the device can be seen in figure 52. Since no difference has been observed between the two internal pressure taps, in the next paragraph only one will be used to present the results. The same holds true for the two external taps.

The device has been measured in two positions corresponding to the areas where there were the highest pressure taps density in tiles A and B. The device in position B has been tested also with the same upstream building that was used in section 3.2.2 and 4.3.4.

5.3 Results

5.3.1 Tile A

Figure 53 recaps the results obtained with the array of pressure taps described in the previous chapters. The plot represents the positive peak, average and negative peak pressure as function of the wind direction for two "classical" pressure taps positioned close to the building's top-corner as well as the same polar curves for the numerically averaged pressure (black lines).

We can see that the two polar curves pressure taps, located only 8mm from

Figure 51: *The device tested in the wind tunnel*

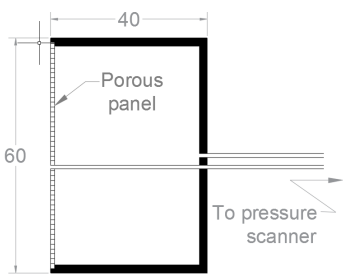

Figure 52: *A section of the device*

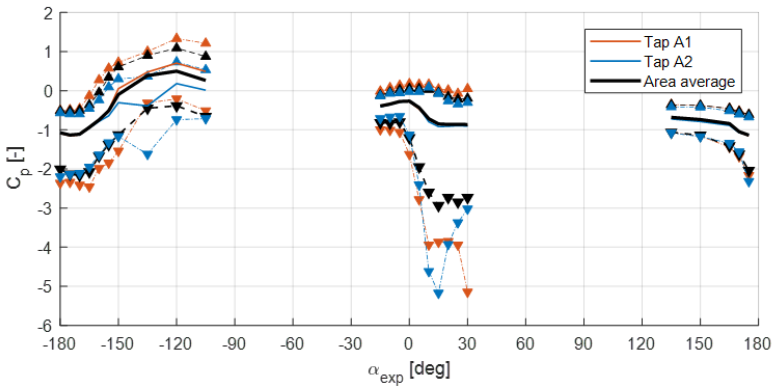

Figure 53: *Positive peak pressure (△), average and negative peak (▽) pressure as function of the wind direction for two "classical" pressure taps and the numerically averaged pressure acting on the top-corner of Tile A*

each other, predicts a peak pressure of $-5.3C_p$ respectively for wind coming from $+10$ degrees and $+30$ degrees. They also predict two different average values for wind coming from -140 degrees, with the blue tap predicting an average pressure of $-0.5C_p$ and the orange one predicting an average pressure of $+0.6C_p$.

When looking at the area-averaged pressure, we can see a much weaker peak pressure for the wind coming from 0 to 30 degrees, with a predicted peak pressure equal to $-3C_p$.

In figure 54 we see the same polar curve of the numerically area-averaged pressure (black line) compared to the results obtained from the pressure measured inside the two versions of the AZA pressure taps. We can see that the analysis of the data measured with both versions of the AZA tap (i.e. the one with 30% porosity and 2mm holes and the one with 10% porosity and 0.5mm holes) predicted both a positive, average and negative peak pressure that is consistent for almost all wind directions with the value obtained using the numerically averaged results. The difference between the peak pressure measured with the AZA taps and the one measured with the array of classical pressure taps is almost everywhere smaller than 0.1 C_p, with only a small shift for wind coming from -120 and -125 degrees.

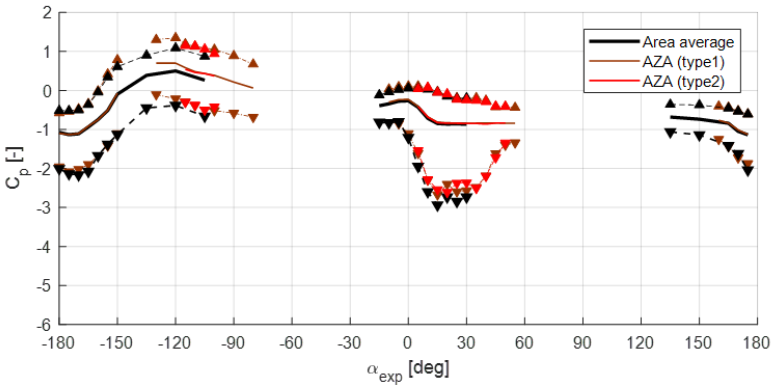

Figure 54: *Positive peak pressure (△), average and negative peak (▽) pressure as function of the wind direction for the numerically averaged pressure and the pressure recorded inside the two AZA taps, acting on the top-corner of Tile A*

5.3.2 Tile B

The same comparison between the results obtained with the numerically averaged data and the one measured within the AZA pressure tap can be performed for the pressure recorded at the mid-height position.

Figure 55 shows the peak values obtained with the single-tap data, the data numerically averaged and the pressure inside the AZA tap. The same comparison has been repeated in figure 56 with an upstream building in order to test the robustness of the technique in different flow conditions.

In both situations, we can see that the AZA taps correctly catches the reduction in the design value obtaining results that perfectly agree with the ones obtained using the numerically-averaged data.

5.3.3 The outer pressure issue

As said in section 5.2, during these test, the pressure was measured both inside the AZA tap and on two points on the external face. The purpose of these pressure taps was to check that the external pressure field remained equal to the pressure field recorded with the aluminium tile and the classical taps. In other words, we want to check if the AZA tap affects in any way the flow outside its panel.

Figure 57 shows a comparison between the pressure recorded inside the AZA

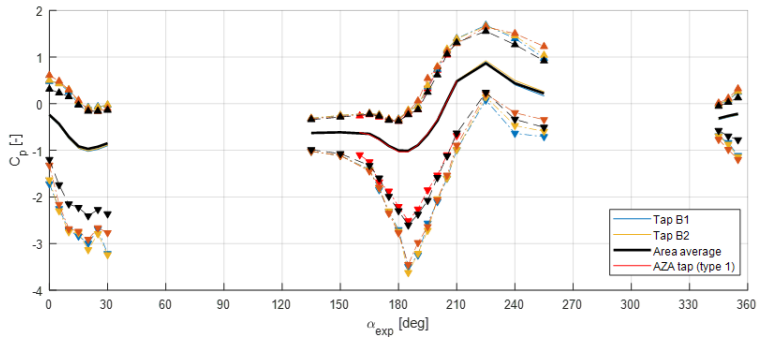

Figure 55: *Positive peak pressure (△), average and negative peak (▽) pressure as function of the wind direction for two "classical" pressure taps, the numerically averaged pressure and the pressure recorded inside the AZA tap acting in the mid area of Tile B*

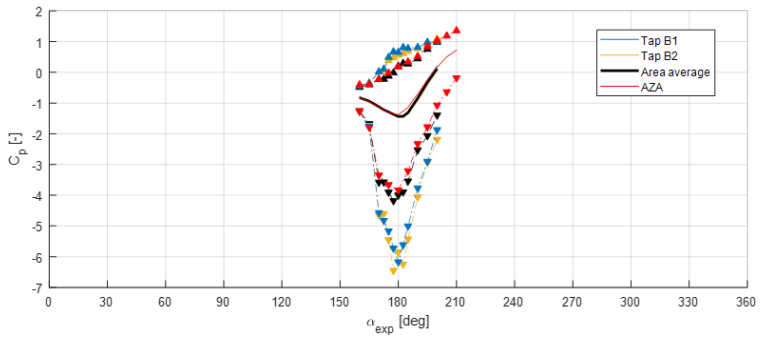

Figure 56: *Positive peak pressure (△), average and negative peak (▽) pressure as function of the wind direction for two "classical" pressure taps, the numerically averaged pressure and the pressure recorded inside the AZA tap acting in the mid area of Tile B with an upstream building*

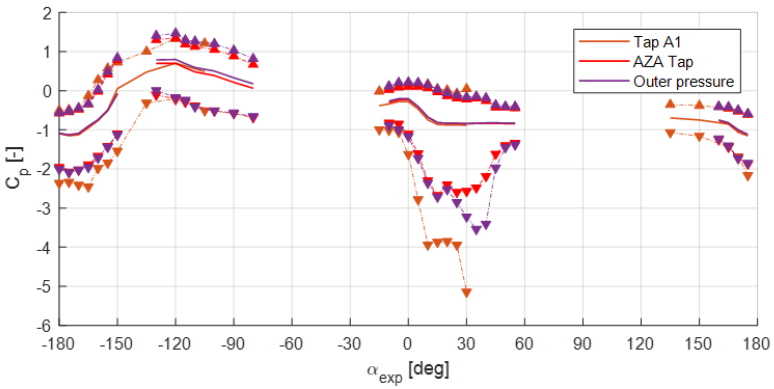

Figure 57: *Positive peak pressure (△), average and negative peak (▽) pressure as function of the wind direction for the pressure recorded inside the AZA tap, outside the AZA tap panel and on the closest "classical" pressure tap of the first stage of testing*

tap, the one recorded on its external surface and the closest classical pressure tap on the aluminium tile. Comparing the negative peak pressure, we can see that for wind coming from 0 to 15 degrees, the pressure recorded by the external tap is almost identical to the pressure measured by the tap inside the AZA tap. For the wind coming from the directions ranging from 15 to 45 degrees, there is a difference between the pressure recorded inside the AZA tap and the one measured on the external surface.

These results seem to suggest that the AZA tap somehow alter the pressure field on the building surface and could, at least in theory, alter the velocity field around the building. It is nonetheless evident however how the area-averaged pressure match in both the test with the array of classical pressure taps and the one with the AZA tap. This suggests that the alteration of the pressure and velocity field, if it exists, is negligible when the area-averaged pressure is observed.

This behaviour should be further studied to understand if and to which degree the presence of the AZA tap is affecting the pressure field.

5.4 Comparison in the frequency domain

One benefit of the measurement of the area-averaged pressure, using the described device is that the signals' spectra can be considered reliable up to the system's maximum sampling frequency and is not affected by any arbitrary filter (e.g. the moving average or another low-pass filter).

This is evident from figure 58 where the spectrum of the pressure inside the AZA tap (red lines) is compared to the spectrum of the numerically area-averaged pressure (black lines) for three different positions and flow conditions. The light blue lines represent the spectrum of the raw signal while the green line represents the spectrum of the signal filtered with a moving-average filter with a span evaluated using the equation $\tau = 4.5\, L/V$.

From this comparison can be evinced that even if the TVL equation in the original Lawson form produce an *almost* correct evaluation of the design peak value (as seen in chapter 4), the spectrum of the signal obtained is obviously severely affected by the filtering operation. On the contrary, the pressure measured behind the porous panel seems able to catch the correct area-averaged pressure's spectrum.

This behaviour can be exploited to take into account the frequency response of the cladding structural system simply multiplying the spectrum of the signal by the FRF of the supporting system.

5.5 Further development

In this chapter we have proposed a simple and economical device that is able to correctly catch the area-averaged pressure acting on a building surface.

At the time of writing this thesis, only the two versions described in section 5.2 have been tested. Before being able to effectively use this new approach on real tests, a real calibration and optimization of the device needs to be performed and some issues need to be addressed.

5.5.1 Parametrization of the design

The design of the AZA tap is very simple and can be described using just three parameters (in addition to the frontal area). In order to achieve the best possible solution, however, their effect needs to be assessed. Hereafter we will shortly summarize them and their expected effect on the device performance

- The first parameter is the **porosity** of the front panel i.e. the ratio between the total holes area and the area of the pressure tap. A low

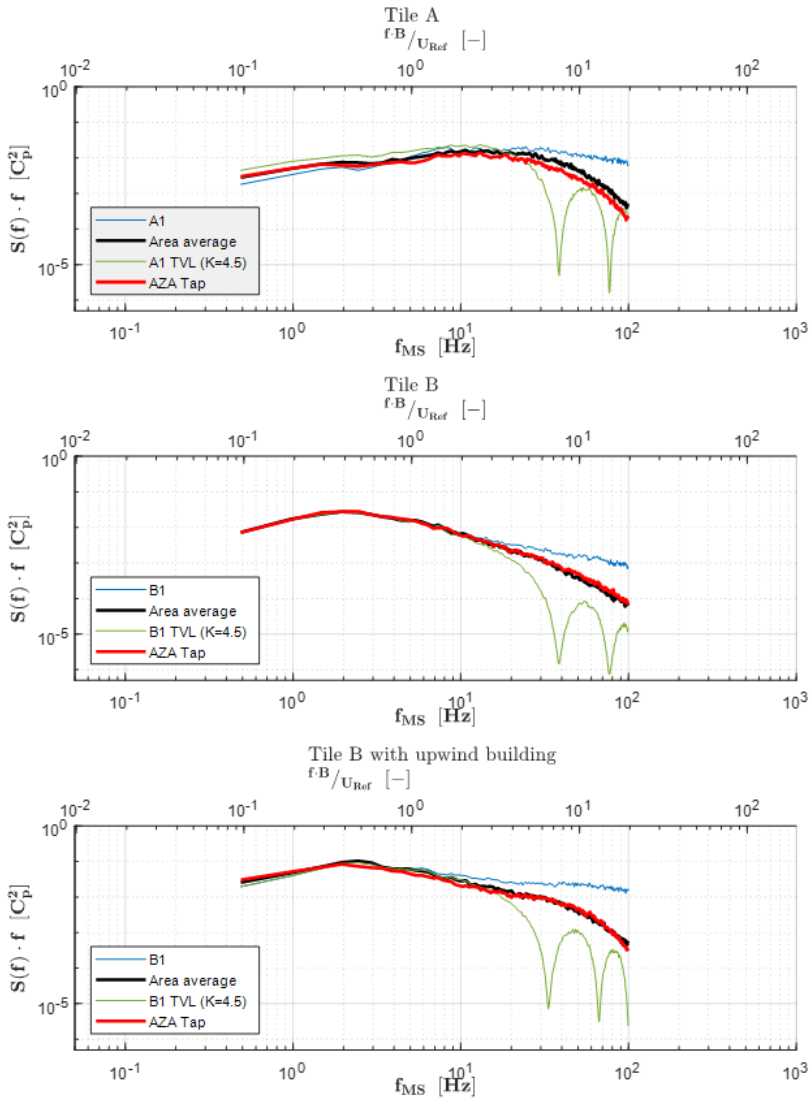

Figure 58: *Comparison between single tap, area-averaged, time-averaged and AZA tap signals' spectra*

porosity value leads to a completely closed front panel. This would obviously hinder the correct behaviour of the device. On the other hand, a porosity whose value tends to 1 means to have a completely open device. In this case the flow pattern outside of the pressure tap will be affected by the cavity on the building surface, altering the model's aerodynamic behaviour and distorting the results.

- The second parameter is the **dimension of the holes** on the front panel. Using holes with a large diameter would mean that the same porosity value will be achieved with a smaller number of holes. This will cause the distribution to not be spatially homogeneous and the average to not be representative of all the points in the same way. On the other hand, a dimension of the holes too small would lead to holes so narrow that the viscous stresses on the holes' lateral surfaces are no longer negligible. This would also cause practical issues in the realization of the panel.
- The last parameter is the **volume** of the internal cavity. Assuming the frontal area to be driven by design choices, the internal volume is directly proportional to the depth of the tap. A volume too big will lead to a bulky and unpractical device. Moreover, it would also lower the resonance frequency, leading to possible measurement errors. A small depth, on the other hand, would cause the rear side of the tap to be very close to the frontal panel. In such situation the pressure inside the cavity would likely not be spatially constant and some doubt arise on the correctness of the results.

For the two tested taps, these three parameters has been chosen with a *reasonable guess*. However, further testing are planned to understand how (or if) these parameters affect the measure and which is the optimal value for each of them.

Another open question relates to the way in which this tap should be scaled when changing the geometrical scale of the test. Being the porosity a dimensionless number, it should not be affected by the scaling. On the other hand, the hole size and the depth of the tap are dimensional value that should, in first instance, be scaled with the model. Some questions arise, however, on if the hole size should be scaled according to the geometrical scale or if, instead, a small hole size can be kept constant for a range of test scales.

5.5.2 A way to take into account the influence surface

In (Holmes, 1997), Holmes highlighted how the current method does not consider the effect of the influence line (or surface for 2D cases) when evaluating

the maximum load or stresses in a structural element.

The influence line is a function expressing which is the value of the effect of interest (e.g. the bending moment in one section, a reaction, etc.) due to a unitary load applied in different point of the structure. Since the wind pressure acting on a surface is never uniform, to correctly evaluate any effect, the pressure at any point should be multiplied by the value of the influence line/surface at the same point. In mathematical terms this can be written as:

$$F = \int_A p(\mathbf{x}_p)\, \eta(\mathbf{x}_p)\, \mathrm{d}A \tag{20}$$

where $\mathbf{x}_p$ is the position on the structure, F is the effect of interest and $\eta(\mathbf{x}_p)$ is the influence surface.

Some examples of influence line for 1D structure is reported in figure 59. Figure 59a represents the influence line for the vertical reaction in the left end of the beam. In this case the loads close to the left end of the beam have a greater effect than the loads on the right end. This should be taken into account when integrating the pressure field, but, despite this, the coefficients are all positive. This means that all the loads give a positive contribution to the effect of interest. In (Holmes, 1997) is shown how using an *effective length* in place of the real characteristic length of the structure can partially solve the issue.

Figure 59b, instead, represents the influence line for the central bending moment of a three-span beam. In this case the influence line contains negative parts. This means that positive pressure on the side spans generate a *reduction* of the bending moment in the central span, while the same positive pressure applied on the central span generates an *increase* of the effect.This behaviour cannot be reproduced with the time-averaging concept and the quasi-steady approach will produce unconservative results.

If we consider a AZA tap and we assume the porosity to be a continuous function over the tap surface, we can rewrite equation 15 in integral form as:

$$p_{AZA} = \frac{1}{\int_A \phi(\mathbf{x})\, \mathrm{d}A} \int_A p(\mathbf{x})\, \phi(\mathbf{x})\, \mathrm{d}A \tag{21}$$

where $\phi(\mathbf{x})$ is the porosity in position $\mathbf{x}$.

If we compare equations 20 and 21 we see that in both cases the function $\eta(\mathbf{x})$ and $\phi(\mathbf{x})$ can be interpreted as a weighting function for the pressure field $p(\mathbf{x})$.

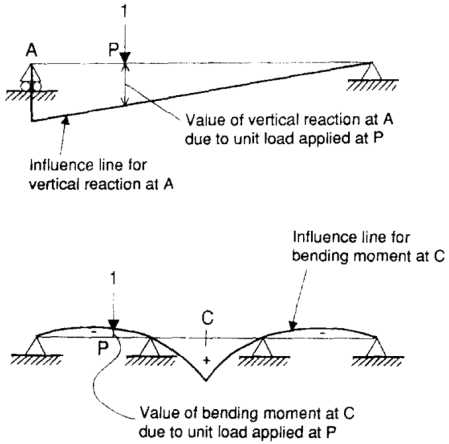

Figure 59: *Example of influence lines for a simply supported beam (from (Holmes, 1997))*

Exploiting this similarity, we can try to create an AZA tap that is able to evaluate the effective pressure weighted for the correct influence line. This can be achieved, for example, varying the diameter of the holes across the surface of the AZA tap respecting the equation of the influence line of interest.

One limitation to this technique, however, is the fact that the function $\phi(\mathbf{x})$ can only be positive and the reproduction of the negative contribution areas could be tricky. One solution could be to have a two AZA tap, one measuring the pressure in the area where it gives a positive contribution to the effect and another in the area where it gives a negative contribution. The difference of the two pressure signal would then be the effective pressure for the computation of the desired effect.

Such technique, at the moment of writing, has not been tested yet and will be tested in an upcoming set of tests to check its validity.

5.5.3 Concluding remarks on the AZA tap

In this chapter we presented an innovative way to measure the pressure on a building surface that can be used to directly estimate the area-averaged pressure value.

The method relies on the use of a small passive device formed by an empty

cavity with a porous plastic panel on the front face. The pressure acting on the front face communicates with the interior of the tap through an array of holes, where is then measured with a traditional pressure scanner. The device does not have any moving, nor electric component and can be easily realised using CNC machinery or 3D printing technology. The frontal panel can also be realised with rather inexpensive technologies. In the current test we used a laser-cut PMMA panel with a cost of less than 1 euro per panel.

The tap can be realised with a circular cross section, for an easier installation on wind tunnel models, or with the same geometry of the real façade panel, for a more precise estimation of the averaged pressure. Moreover, we proposed a solution to measure the pressure field spatially averaged with an arbitrary weighting function. This could be used, for example, to take into account the influence surface of a quantity of interest.

The solution has been tested in two different positions on the building. Moreover, both the stand-alone configuration and the one within the wake of an upwind building have been tested. The results were compared with the ones obtained from the measurement of the pressure field with 72 independent "classical" pressure taps numerically averaged.

In all the situations the proposed device worked remarkably well, being able to catch both the mean and peak value, and the correct spectrum of the area-averaged pressure.

Some questions still exist on the device. At the current stage of the research there is no information regarding if or how its geometry could affect the results. The parameters whose effect should be studied include the porosity of the front panel, the hole size and the internal volume of the tap.

Another question is whether or not the presence of the tap could alter the pressure field around the building. The results obtained in this stage of the research are somehow contradictory: the pressure tap on the outside of the porous panel of the AZA tap recorded a pressure level more similar to the one inside the porous panel itself, then the one that was expected on the "naked" building surface; however, the level of precision with which the AZA tap is able to reproduce the area-averaged pressure measurement seems to suggest the effect of the tap on the pressure field is negligible.

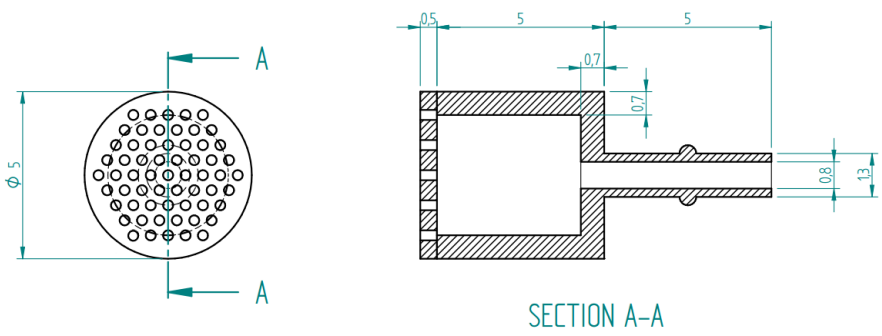

Figure 60: *A possible operative version of the AZA tap*

Chapter 6

Conclusions

In this thesis we presented the results of an experimental high-resolution survey of the space-time distribution of the wind-induced pressure field acting on a wind tunnel model.

The purpose of the research was to study the correct way to post-process the pressure time-histories recorded in a wind tunnel experiment in order to produce the most accurate design value for the cladding design. Special attention was paid to the "sharp" suction peaks responsible for the strong skewness measured in some critical areas of the building. These peaks represent for many position the most adverse events and they are directly responsible for the design value in those regions. Due to the short duration, however, they are strongly affected by any time-filtering technique. Since a physical explanation of the cause of these events is still elusive, the correctness of such time-filtering approach was disputed.

In chapter 3, exploiting the high spatial resolution used in this research, we have been able to study the relationship between the duration and the spatial size of these events. It has been observed that the correlation between the duration and the size of this events is poor in many areas, raising doubts regarding the equivalence between time and space filtering.

The study of the proportionality parameter between the duration and the size of the phenomena, highlighted that the median value of such parameter is not far from the value predicted by the current state-of-the-art. Its dispersion, however, and the fact that the median value can significantly change depending on several factors (such as the portion of the building considered, the wind direction or the presence of the surrounding) proved how the time-averaging approach , adopting the same equation for whatever situation (exposure, sur-

rounding, geometry, etc.), cannot be considered rigorous.

At this point should be highlighted that this research never aimed at a physical understanding of the phenomenon responsible for the generation of these peak events. However, having observed in some small areas of the building surface some extreme events very different from the ones predicted by the current physical understand of the phenomenon, it's the authors opinion that a possible future line of research could aim at the study of the velocity field generating such events.

These events, however, has been observed in an area where the flow is strongly three-dimensional and they are characterized by a duration in the order of the hundredth of second and a spatial size in the order of the millimetre. Such characteristics make them difficult to be studied with both experimental and numerical techniques.

A CFD simulation aimed at the reproduction of such events should obviously be unsteady. This excludes the RANS techniques. An LES (or DNS) simulation should have, at least locally, a spatial resolution higher than 1 millimetre. Considering a reference velocity of 10 m/s, in order to respect the CFL condition the time-step should be smaller than 1/10'000 seconds. These requirements, together with a domain in the order of tens of cubic metres, make the computational cost of such simulation extremely high and out-of-reach for current ordinary HPC.

Despite the above mentioned consideration on the relationship between the duration of the events and their size, in the wind-tunnel practice the time-filtering of the pressure data is a consolidated habit. Moreover, nowadays no real alternative exists. In chapter 4 we tried to quantify the error that different time-filtering technique make when applied to single-tap data.

It turns out that despite the observations of chapter 3, the error made using a moving average filter with a span evaluated with the Lawson's TVL equation (i.e. $\tau = 4.5L/V$) is smaller than 1 C_p for most areas, while a moving average with a span evaluated with the TVL equation in the form $\tau = L/V$ produces design values that are generally over-conservative.

This finding seems to suggest that the large dispersion of the K value described in section 3.3 could be driven by non-dimensioning peaks and that, if we limit our study only to these, the dispersion in the distribution decrease.

While this conclusion is valid for most areas and most flow situations, in some small portion of the building surface where the most extreme pressure peaks have been observed the design value obtained filtering the pressure time-histories with the moving average prescribed by Lawson still generates design

value that are up to 3 C_p higher than the area-averaged pressure time-history.

One future development to improve the performance of the TVL equation is to study a possible parametrization of the constant K. This could lead to an equation tuned for different flow situations (windward face, leeward, separation bubble, etc) and for different geometries, without losing its ease of use. This would allow a more conscious use of the TVL equation.

In chapter 5 an experimental solution for a more robust evaluation of the area-averaged pressure has been proposed. Since the "averaging" operation is performed by the physics of the device itself, the need of an analytical evaluation of the spatial correlation of the pressure from a single time-history is completely eliminated.

The results showed that the peak value evaluated with the proposed device match the one evaluated with the area-averaged array of pressure tap with an error that is almost everywhere lower than $0.25C_p$. The proposed method has also the advantage that produce a signal whose spectrum match the spectrum of the one of the area averaged pressure up to the maximum sampling frequency allowing the characterization not only of the mean and peak pressure, but it's whole frequency content.

Since the results are very promising, future tests will be aimed at the characterization of the proposed solution in different positions and flow conditions and at the study of the optimal geometry of the device.

Bibliography

Banks, D., R. Meroney, P. Sarkar, Z. Zhao, and F. Wu (2000, January). Flow visualization of conical vortices on flat roofs with simultaneous surface pressure measurement. *Journal of Wind Engineering and Industrial Aerodynamics 84*(1), 65–85.

Bearman, P. W. (1971, March). An investigation of the forces on flat plates normal to a turbulent flow. *Journal of Fluid Mechanics 46*(01), 177.

Calderone, I. and W. Melbourne (1993, September). The behaviour of glass under wind loading. *Journal of Wind Engineering and Industrial Aerodynamics 48*(1), 81–94.

Cook, N. J. (1985). *The Designer's Guide To Wind Loading Of Building Structures - Part1*. Butterworths (for) Building Research Establishment, Department of the Environment, London.

Cook, N. J. (1990). *The Designer's Guide to Wind Loading of Building Structures - Part 2: Static structures*. Building Research Establishment Report. Building Research Establishment, Department of the Environment.

Cook, N. J. and J. R. Mayne (1979, March). A novel working approach to the assessment of wind loads for equivalent static design. *Journal of Wind Engineering and Industrial Aerodynamics 4*(2), 149–164.

Davenport, A. G. (1961). The application of statistical concepts to the wind loading of structures. *ICE Proceedings 19*(4), 449–472.

Davenport, a. G. (1964). the Buffeting of Large Superficial Structures By Atmospheric Turbulence. *Annals of the New York Academy of Sciences 116*(1), 135–160.

Gavanski, E. and Y. Uematsu (2014, September). Local wind pressures acting on walls of low-rise buildings and comparisons to the Japanese and US wind loading provisions. *Journal of Wind Engineering and Industrial Aerodynamics 132*, 77–91.

Greenway, M. E. (1979). An analytical approach to wind velocity gust factors. *Journal of Wind Engineering and Industrial Aerodynamics 5*(1-2), 61–91.

Harris, R. I. (2009). XIMIS, a penultimate extreme value method suitable for all types of wind climate. *Journal of Wind Engineering and Industrial Aerodynamics 97*(5), 271–286.

Holmes, J. D. (1997, November). Equivalent time averaging in wind engineering. *Journal of Wind Engineering and Industrial Aerodynamics 72*, 411–419.

Holmes, J. D. and A. Allsop (2013). Gust durations and effective frontal areas – with applications to codes and standards.

Huang, P., X. Peng, and M. Gu (2014, December). Aerodynamic devices to mitigate rooftop suctions on a gable roof building. *Journal of Wind Engineering and Industrial Aerodynamics 135*, 90–104.

Lawson, T. (1980). *Wind effect on buildings, Volume 1: Design applications*. London: Applied Science Publishers.

Lawson, T. V. (1976, January). The design of cladding. *Building and Environment 11*(1), 37–38.

Lin, J. and D. Surry (1998). The variation of peak loads with tributary area near corners on flat low building roofs. *Journal of Wind Engineering and Industrial Aerodynamics 77*, 185–196.

Lin, J., D. Surry, and H. W. Tieleman (1995, May). The distribution of pressure near roof corners of flat roof low buildings. *Journal of Wind Engineering and Industrial Aerodynamics 56*(2-3), 235–265.

Newberry, C. W., K. J. Eaton, J. R. Mayne, and B. R. Establishment (1974). *Wind loading on tall buildings : further results from Royex House*. Watford : Building Research Establishment. Published in Industrial Aerodynamics Abstracts, Vol. 4, No. 4, July-August 1973.

Ono, Y., T. Tamura, and H. Kataoka (2008, October). LES analysis of unsteady characteristics of conical vortex on a flat roof. *Journal of Wind Engineering and Industrial Aerodynamics 96*(10-11), 2007–2018.

Peng, X., L. Yang, E. Gavanski, K. R. Gurley, and D. O. Prevatt (2014, March). A comparison of methods to estimate peak wind loads on buildings. *Journal of Wind Engineering and Industrial Aerodynamics 126*, 11–23.

Randeberg, R. T. (2000). *Perforated Panel Absorbers with Viscous Energy Dissipation Enhanced by Orifice Design*. Doctoral thesis, NTNU.

Rocchi, D., P. Schito, and A. Zasso (2010). Evaluation of unsteady pressure fluctuations on surfaces using CFD. In *The Fifth International Symposium on Computational Wind Engineering (CWE2010)*, pp. 1–8.

Rocchi, D., P. Schito, and A. Zasso (2011). Investigation on the relation between incoming wind characteristics and surface pressure distribution.

Schito, P., S. Giappino, A. Zasso, and C. Gorlé (2013). Uncertainty quantific-

ation of peak pressure loads on a rectangular building. In *6th European and African Conference on Wind Engineering, EACWE 2013*.

Surry, D. and T. Stathopoulos (1978). An experimental approach to the economical measurement of spatially-averaged wind loads. *Journal of Wind Engineering and Industrial Aerodynamics 2*(4), 385–397.

Vickery, B. (1967). Discussion of Reference 1. In *(2nd ed.), Proc. Int. Res. Seminar on Wind Effects on Buildings and Structures, Ottawa, Vol. 2*, Ottawa, pp. pp. 413–426.

Wu, F. (2000a). Full-Scale Study of Conical Vortices and Their Effects near Roof Corners. *Wind and Structures 4*(2), 131–146.

Wu, F. (2000b). *Full-scale study of conical vortices and their effects near roof corners (Ph.D. Thesis)*. Ph.d. dissertation, Texas Tech University.

Wu, F., P. Sarkar, K. Mehta, and Z. Zhao (2001, April). Influence of incident wind turbulence on pressure fluctuations near flat-roof corners. *Journal of Wind Engineering and Industrial Aerodynamics 89*(5), 403–420.